

# Glueballs and $k$ -strings in $SU(N)$ gauge theories : calculations with improved operators

Biagio Lucini<sup>a</sup>, Michael Teper<sup>b</sup> and Urs Wenger<sup>c</sup>

<sup>a</sup>Institute for Theoretical Physics, ETH Zürich,  
CH-8093 Zürich, Switzerland

<sup>b</sup>Theoretical Physics, University of Oxford,  
1 Keble Road, Oxford OX1 3NP, U.K.

<sup>c</sup>NIC/DESY Zeuthen, Platanenallee 6, 15738 Zeuthen, Germany

## Abstract

We test a variety of blocking and smearing algorithms for constructing glueball and string wave-functionals, and find some with much improved overlaps onto the lightest states. We use these algorithms to obtain improved results on the tensions of  $k$ -strings in  $SU(4)$ ,  $SU(6)$ , and  $SU(8)$  gauge theories. We emphasise the major systematic errors that still need to be controlled in calculations of heavier  $k$ -strings, and perform calculations in  $SU(4)$  on an anisotropic lattice in a bid to minimise one of these. All these results point to the  $k$ -string tensions lying part-way between the ‘MQCD’ and ‘Casimir Scaling’ conjectures, with the power in  $1/N$  of the leading correction lying  $\in [1, 2]$ . We also obtain some evidence for the presence of quasi-stable strings in calculations that do not use sources, and observe some near-degeneracies between (excited) strings in different representations. We also calculate the lightest glueball masses for  $N = 2, \dots, 8$ , and extrapolate to  $N = \infty$ , obtaining results compatible with earlier work. We show that the  $N = \infty$  factorisation of the Euclidean correlators that are used in such mass calculations does not make the masses any less calculable at large  $N$ .

# 1 Introduction

Consider a lattice with spatial and temporal lattice spacings  $a_s$  and  $a_t$  (generically referred to as  $a$  when equal). Monte Carlo calculations of the eigenvalues of the Hamiltonian,  $H$ , usually proceed via the calculation of Euclidean correlation functions

$$C(t) = \langle \Phi^\dagger(t)\Phi(0) \rangle = \sum_n |\langle \Omega | \Phi^\dagger | n \rangle|^2 e^{-E_n t} = \sum_n |c_n|^2 e^{-a_t E_n n t} \quad (1)$$

where

$$H|n\rangle = E_n|n\rangle, \quad (2)$$

and  $t \equiv a_t n_t$ . If we were interested in a glueball mass, we would construct  $\Phi$  from products of link matrices around closed contractible loops, and we would take linear combinations such that  $\Phi$  has the appropriate  $J^{PC}$  quantum numbers and  $\vec{p} = 0$ . To calculate the tension of a  $k$ -string we would use a non-contractible loop that winds  $k$  times around a spatial torus. (See Section 3.1 and e.g. [1, 2] for more details.)

Suppose we are interested in the mass of the state  $|l\rangle$ . Since the statistical errors in these calculations are approximately independent of  $t \equiv a_t n_t$  while, as we see from eqn(1), the desired ‘signal’ drops exponentially in  $n_t$ , it is clearly important to construct operators that have  $|c_l|^2 \simeq 1$  (normalising to  $\sum |c_n|^2 = 1$ ) if the contribution we are interested in,  $|c_l|^2 e^{-a_t E_l n t}$ , is to dominate at the small values of  $n_t$  where it is still much larger than the errors. That is to say, we need an operator  $\Phi$  that is a good approximation to the wave-functional of the state  $|l\rangle$ . This is more important the heavier the state.

Simple loops of bare fields are highly local and will project more-or-less equally on all states. Operators that project mainly on the lightest physical states should be smooth on the ultraviolet lattice scale. Fast iterative techniques for constructing such operators go under the names of blocking [3] and smearing [4]. Although the existing techniques have allowed for the accurate calculation of the lightest masses, even at small  $a$ , they are not good enough in all cases. In particular, the overlaps of  $k$ -strings are found [1] to satisfy

$$|c_k|^2 \simeq \left\{ |c_{k=1}|^2 \right\}^k \quad (3)$$

and the mass of the string increases rapidly with  $k$ . Thus an acceptable overlap for the fundamental string, e.g.  $|c_{k=1}|^2 \sim 0.85$ , transforms into a uselessly poor overlap for, say, a  $k = 4$  string.

In this paper we suggest and test some improvements to the common blocking and smearing techniques. Using these improved methods we present some illustrative calculations of  $k$ -string tensions and glueball masses for groups as large as SU(8).

Using anisotropic lattices with  $a_t \ll a_s$  provides a finer resolution of the  $t$ -dependence of  $C(t)$  and helps to establish the minimum  $t$  at which the lightest mass already dominates  $C(t)$  [5]. This is of particular importance for heavy masses, such as those of  $k$ -strings with  $k > 1$ , where it is undoubtedly the source of the major systematic error in current calculations. We

perform calculations of  $k = 2$  string tensions in  $SU(4)$  using anisotropic lattices with the emphasis on minimising this particular systematic error.

All these calculations obtain masses from correlations of field fluctuations. However we know that in the  $N = \infty$  limit there are no fluctuations and correlators factorise. One might wonder if this means that mass calculations become impossible as  $N \rightarrow \infty$ <sup>1</sup>. We analyse this question towards the end of this paper.

In the next section we summarise the lattice ‘setup’. We then move on to discuss systematic errors, with the focus on those that are potentially important in calculations of  $k$ -string tensions. The following section embellishes the standard blocking and smearing algorithms, with detailed numerical tests to establish the extent of the improvement. We then summarise the results of our calculations with these improved operators, as well as some with an anisotropic lattice spacing, first for glueballs and then for  $k$ -strings, where we demonstrate how improving the operators has improved upon previous work. In addition to the lightest, stable  $k$ -strings we observe evidence for heavier, quasi-stable strings. Finally, after a general analysis of mass calculations in the  $N \rightarrow \infty$  limit, we summarise, in the concluding section, what we have learned about the physics, the methods, and what are some of the outstanding problems.

## 2 Lattice setup

We use hypercubic, periodic lattices of size  $L_s^3 L_t$  (using  $L$  when there is no ambiguity). We assign  $SU(N)$  matrices,  $U_l$ , to the links  $l$ . (Or equivalently  $U_\mu(n)$  for a link emanating in the  $\mu$  direction from site  $n$ .) For most of our calculations we use the standard isotropic ( $a_s = a_t = a$ ) plaquette action

$$S = \beta \sum_p \left\{ 1 - \frac{1}{N} \text{ReTr} U_p \right\}, \quad (4)$$

where  $U_p$  is the ordered product of the  $SU(N)$  matrices around the boundary of the plaquette  $p$ .  $S$  appears in the Euclidean Path Integral as  $e^{-S}$  and becomes, in the continuum limit, the usual Yang-Mills action with

$$\beta = \frac{2N}{g^2}. \quad (5)$$

As we vary  $N$  we expect [6, 7] that we will need to keep constant the ‘t Hooft coupling,  $\lambda$ ,

$$\lambda \equiv g^2 N \quad (6)$$

for a smooth large- $N$  limit. Non-perturbative calculations [1, 2] support this expectation.

The anisotropic lattice action we use is

$$S = \beta_s \sum_{p_s} \left\{ 1 - \frac{1}{N} \text{ReTr} U_{p_s} \right\} + \beta_t \sum_{p_t} \left\{ 1 - \frac{1}{N} \text{ReTr} U_{p_t} \right\} \quad (7)$$

---

<sup>1</sup>We are grateful to Simon Dalley for making this point to one of us a number of years ago.

where  $p_s$  and  $p_t$  are spatial and temporal plaquettes, and the couplings are related to the anisotropy

$$\xi = \frac{a_t}{a_s} \quad (8)$$

by

$$\beta_s = \xi\beta \quad ; \quad \beta_t = \frac{1}{\xi}\beta \quad ; \quad \beta = \frac{2N}{g^2} \quad (9)$$

at tree level. The actual renormalised anisotropy,  $\xi_r$ , will differ from the bare anisotropy,  $\xi = \sqrt{\beta_s/\beta_t}$ , that we use in eqn(9) in setting the couplings. If we were only interested in ratios of masses this would not matter: we can safely extrapolate  $a_t m_a / a_t m_b \equiv m_a / m_b$  to the continuum limit with an  $(a_t m_c)^2$  correction term. However if we wish to calculate a string tension this is no longer so since the mass,  $m_k$ , of the winding  $k$ -string is given by

$$a_t m_k = a_t a_s L_s \sigma_k - \frac{a_t \pi}{a_s 3L_s}. \quad (10)$$

Here we include the leading long distance string correction [8] to the linear term. So to calculate  $a_t \sqrt{\sigma_k}$  we need to calculate the renormalised anisotropy  $\xi_r = a_t / a_s$ . We shall do so by calculating string energies for the lowest few non-zero momenta and assuming the continuum dispersion relation, as described in detail in Appendix D of ref [9]. Different ways of calculating  $\xi_r$  will differ by lattice spacing corrections, but this will not matter if we perform a continuum extrapolation.

Our simulations are performed with a combination of heat bath and over-relaxation updates, as described in [1, 2]. We update all the  $N(N-1)/2$  SU(2) subgroups of the SU( $N$ ) link matrices.

## 3 Systematic errors

### 3.1 k-strings

What is a  $k$ -string? Consider sources that transform as  $\psi(x) \rightarrow z^k \psi(x)$  under a global gauge transformation in the centre of the group,  $z \in Z_N$ . Gluon screening cannot change  $k$  but can change one source to another of the same  $k$ . The  $k$ -string is the flux tube with the smallest string tension in the  $k$  class, and so it is a stable string. All other strings in the  $k$  class will decay to it (for a long enough string). One finds [1] that it corresponds to the totally antisymmetric representation. Obvious constraints arise from  $z^N = 1$  and from the fact that  $k$  and  $-k$  are charge conjugates. So for  $N \leq 3$  we only have  $k = 1$  strings, for  $N \geq 4$  we also have  $k = 2$  strings etc.

We expect

$$\sigma_k \xrightarrow{N \rightarrow \infty} k\sigma \quad ; \quad \sigma \equiv \sigma_{k=1} \quad (11)$$

and the interesting physical question is how tightly bound are the  $k$ -strings at finite  $N$ . Earlier calculations [1, 10] have established that the values of  $\sigma_k/\sigma$  lie in the range spanned by the

‘Casimir Scaling’ [11] and ‘MQCD’ [12] conjectures

$$\frac{\sigma_k}{\sigma} = \begin{cases} k(N-k)/(N-1) & : \text{‘Casimir scaling’} \\ \sin \frac{k\pi}{N} / \sin \frac{\pi}{N} & : \text{‘MQCD’} \end{cases} \quad (12)$$

(See [1, 10] for a more detailed discussion.) To be able to firmly exclude one or both of these possibilities requires an accuracy at the  $\leq \pm 2\%$  level on  $\sigma_k$ . There are at least two sources of systematic error that can be significant at this level of precision. The first tends to lead to the value of  $\sigma_k/\sigma$  being overestimated, and increasingly so for increasing  $k$  and  $N$ . The second works (potentially) in the reverse direction.

### 3.1.1 extracting the mass

When we estimate a mass from the correlator in eqn(1) we do so by calculating the effective masses

$$am_{eff}(t) = -\ln \frac{C(t)}{C(t-a)} \quad (13)$$

and identifying an effective mass plateau  $t \geq t_{min}$  where  $am_{eff}(t_{min}) = am_{eff}(t)$ ,  $t \geq t_{min}$ , within errors. Thus for  $t \geq t_{min}$  we can regard  $C(t)$  as being given by a single exponential and we can then use  $am_{eff}(t_{min})$  as our estimate of the actual mass. (The actual procedure will typically involve fits over ranges of  $t$ , but this does not alter the argument.) Now, since  $\sigma_k$  grows with  $k$  (and indeed with  $N$ ) the mass of the corresponding string also grows. For such heavy states the correlator in eqn(1) drops rapidly into the statistical noise as we increase  $t$  and the significance of an apparent effective mass plateau decreases. Thus for heavier states we will typically end up extracting the mass at a value of  $t$  that is too low. Given the positivity of the correlator, this means that the mass estimate will be somewhat too high. This shift will grow with  $k$  because the mass grows with  $k$ . It is thus a systematic bias that will lead to an overestimate of  $\sigma_k/\sigma$ , and the overestimate will increase with  $k$  and  $N$ . Since an increase in statistical errors has the same type of effect, if the higher  $N$  calculations have lower statistics (which can easily happen because they are more expensive) this systematic bias will be further enhanced. This is further compounded by the fact that the overlap of the best operator typically decreases with  $k$ , as in eqn(3), so that the real value of  $t_{min}$  is higher for these more massive states.

The solution to this problem is firstly to find improved operators for which  $|c_{k=1}|^2 \simeq 1$  so that  $|c_k|^2 \sim 1$  for the values of  $k$  of interest; secondly to find methods that can improve the statistical accuracy of calculations of heavier masses at larger  $n_t$ . Once this is done, calculations with anisotropic lattices may be very useful in giving us a finer-grain in  $t$  so that we can establish the existence of a plateau with greater certainty.

In this paper we go some way to providing the first part of this solution, showing how one can significantly improve operator overlaps in a simple way. We do not address the second part, on how to improve the statistical accuracy of mass calculations of heavy states, but note that important progress has very recently been made on this problem [13] in a generalisation of the recent multi-level algorithm for Wilson loops [14]. Finally, we perform a limited anisotropic lattice calculation to illustrate its utility.

### 3.1.2 finite volume correction

Denoting the lightest mass of a periodic  $k$ -string of length  $l = aL$  by  $m_k(L)$ , we expect [8, 1] that at sufficiently large  $l$  we will have

$$am_k(L) \equiv a^2\sigma_k(L)L = a^2\sigma_k(\infty)L - \frac{\pi}{3L} \quad (14)$$

up to higher order corrections in  $1/L^2$ . There is good evidence that this has become a very accurate approximation to  $k = 1$  strings once  $aL\sqrt{\sigma} \geq 3$  [1], but the evidence that this is also so for  $k > 1$  strings [1] is very much less precise. Current calculations of  $k$ -string tensions are with  $aL\sqrt{\sigma} \sim 3$  and assume the validity of eqn(14). This raises an important issue because the magnitude of the shift in  $\sigma_k/\sigma$  produced by, for example, doubling the  $O(1/L^2)$  correction to  $\sigma_k(L)$  is typically as large (or larger than) the difference between the two possibilities in eqn(12).

Theoretically, there is something one can say about these corrections. As  $N \uparrow$  we expect  $\sigma_k \rightarrow k\sigma$  so that the  $k$ -string is less and less strongly bound. Now, the lightest energy of the unbound state composed of  $k$  independent fundamental  $k = 1$  strings is

$$a\tilde{m}_k(L) = kam_{k=1}(L) = ka^2\sigma(\infty)L - k\frac{\pi}{3L} \quad (15)$$

for large enough  $L$ . Because of the larger string correction, this may be lighter than the  $k$ -string bound state for smaller  $L$  and may therefore be the  $k$ -string ground state whose mass we are calculating numerically. One can crudely estimate the critical length  $L_c$  below which this should be so, as the length at which  $a\tilde{m}_k(L)$  in eqn(15) and  $am_k(L)$  in eqn(14) are equal, i.e.

$$a\sqrt{\sigma}L_c(k; N) = \begin{cases} \sqrt{\frac{\pi}{3} \frac{N-1}{k}} & : \text{‘Casimir scaling’} \\ \frac{N}{k} \sqrt{\frac{2}{\pi(1+\frac{1}{k})}} & : \text{‘MQCD’} \end{cases} \quad (16)$$

for the two possibilities in eqn(12), and, in the second case, taking into account only the leading large- $N$  correction. Thus if we calculate  $\sigma_k$  from strings of length  $L < L_c(k, N)$  then we can expect to obtain an underestimate of  $\sigma_k/\sigma$ . We note that for  $k = 2$  and  $N = 8$ , we have  $a\sqrt{\sigma}L_c \sim 2$ . This is getting uncomfortably close to the kind of volume we work on, given the crude and asymptotic nature of the estimate and the fact that there may well be an extended transition region between the unbound and bound states.

One should also consider scenarios where the  $k$ -string is composed of a mixture of  $k' < k$  strings. And given that all these strings of length  $L$  are on a transverse two torus of dimension  $L \times L$  there will be some energy shift for smaller  $L$ . Nonetheless it is clear that if eqn(14) is to be valid for  $k \geq 2$  strings, we will, at large  $N$ , have to go to larger  $L$  than is needed for  $k = 1$  strings, and the systematic bias in not doing so appears to underestimate the value of  $\sigma_k/\sigma$ . Thus it is important to do a much more accurate finite volume study than any currently available. Such a study will involve longer and thus heavier  $k$ -strings and will undoubtedly require something like the multilevel algorithm [13] to be possible. Until such studies are performed any attempt to calculate the  $k$ -string tensions at the few percent level, as we are trying to do when we wish to differentiate between Casimir Scaling and MQCD, must be considered provisional.

### 3.1.3 topology and ergodicity

As  $N$  increases (and also as  $a$  decreases) the lattice fields are increasingly trapped in a given topological charge sector. This is because of the well-known suppression of small instantons at large  $N$  [2, 15, 16, 17]. Thus in SU(8) our sequence of 45000  $16^4$  lattice fields at  $\beta = 45.7$  never changes from  $Q = 0$ . And our 50000  $12^4$  SU(8) fields at  $\beta = 44.85$  only have a very few changes of  $Q$ . Is our volume large enough that the effect of this loss of ergodicity in the global topology on the calculated masses is negligible, or not?

To answer this question we separate our sequence of SU(8) lattice fields at  $\beta = 44.85$  into subsequences with  $Q \simeq 0$ ,  $|Q| = 1$  and  $|Q| \simeq 2$ . (The ‘ $\simeq$ ’ indicates that the subsequences contain a very few fields with a different  $Q$ .) Within these subsequences we perform calculations of the lightest  $k = 1$  and  $k = 2$  string masses, and we list these values in Table 1. We see that the masses appear to be unaffected by the constraint of being in a fixed topological charge sector. This reassures us that, at the level of our precision in this paper, this is not a significant source of error. However this is something that will need checking again if one is doing a much more accurate calculation, and for calculations of other physical quantities.

## 3.2 glueballs

The problems with calculating heavier glueball masses are much the same as for  $k$ -strings and the solution will be similar. It is perhaps less pressing here because there is little demand at present for theoretical comparisons that require accuracy at the percent level. (Except perhaps in recent work on the Pomeron [18].) So, just as for the strings, we will construct improved operators and will provide a calculation on anisotropic lattices. For basic improvements in the Monte Carlo algorithm we refer to [13].

The finite volume issue is much less pressing here because the leading corrections at large volume are exponentially small. Moreover, in contrast to the case of  $k$ -strings, checking for finite volume effects is straightforward because glueballs do not become very heavy on large volumes. So the cost of the calculation is merely linear in the volume – and less so if one calculates the energies corresponding to the lowest non-zero momenta as well.

The one troublesome finite volume effect which occurs on the intermediate spatial sizes that ones uses in practice, comes from a pair of (mutually conjugate) flux loops which can have a non-zero overlap onto glueballs states. In particular in our calculation the mass of such a pair of loops is close to that of the  $0^{+++}$  and we suspect that the frequently poor continuum fits for this state are a sign of mixing between the true  $0^{+++}$  and this finite-volume state (whose mass will diverge in the thermodynamic limit). This can be dealt with by including explicitly operators for such two loop states in the basis so as to identify states which mix with it. Similarly, if one is interested in heavier glueballs and wishes to exclude scattering states of the same quantum numbers, it would be useful to include explicitly operators for such scattering states in the basis. We do not do so in the present paper. We note that the overlaps between such scattering states and the real glueballs should vanish as  $N \rightarrow \infty$  by the usual large- $N$  arguments.

Finally we note in Table 1 that the scalar glueball does not appear to be affected by

constraining the total topological charge  $Q$  to be constant, so we can assume that our mass calculations are not affected by this loss of ergodicity.

## 4 Improved operators

### 4.1 algorithms

In a gauge-invariant lattice calculation, glueball and string operators are composed of ordered products of link matrices around closed loops. If  $a$  is small then we would expect that a good wave-functional for any of the lightest states will be smooth on scales of the order of an appropriate physical length scale and so certainly smooth on the scale of  $a$ . One can achieve this by summing over paths between sites and using these, rather than the original link matrices, as the basic components of the operator. By iterating the procedure one can efficiently sum vast numbers of paths, producing operators smooth on physical length scales.

Traditionally there have been two common variants of this procedure, often referred to as ‘blocking’ [3] and ‘smearing’ [4] respectively. We only consider loops and links that are space-like, so that the positivity of correlation functions is preserved. Thus all indices will run from 1 to 3.

The first step of the usual smearing algorithm sums up the five shortest paths between neighbouring sites, i.e. the link  $l$  and the ‘staples’ (with some relative weighting  $p_a$ ). This produces an  $N \times N$  matrix,  $\tilde{U}_l^{s=1}$ , which we assign to that link, after first projecting it to a ‘nearby’  $SU(N)$  matrix,  $U_l^{s=1}$ . We iterate the procedure

$$\begin{aligned} \tilde{U}_i^{s+1}(n) &= U_i^s(n) + p_a \sum_{j \neq i} U_j^s(n) U_i^s(n + \hat{j}) U_j^{s\dagger}(n + \hat{i}) \\ &\quad + p_a \sum_{j \neq i} U_j^{s\dagger}(n - \hat{j}) U_i^s(n - \hat{j}) U_j^s(n - \hat{j} + \hat{i}), \\ U_i^{s=0}(n) &= U_i(n) \end{aligned} \tag{17}$$

with

$$U_i^{s+1}(n) = \mathcal{U} \left\{ \tilde{U}_i^{s+1}(n) \right\} \tag{18}$$

representing the procedure by which the matrix is transformed into a special unitary one. We can now form operators by multiplying these smeared link matrices around closed loops  $c$

$$\Phi(\mathcal{C}) = \sum_{c \in \mathcal{C}} \prod_{l \in c} U_l^s \tag{19}$$

where it is understood that if we go backward along a link  $l$  then we use  $U_l^{s\dagger}$  in place of  $U_l^s$ . The collection of loops  $\mathcal{C}$  can be chosen so as to give the wave-function  $\Phi(\mathcal{C})$  the desired quantum numbers.

Smearing produces  $SU(N)$  matrices on the original links of the lattice. The parameter  $p_a$  determines how rapidly the link field spreads outwards as the procedure is iterated. Choosing

$p_a$  small means that very many smearing steps will be needed to produce links smeared on the desired physical length scale and this will be expensive. On the other hand this will produce operators that extend, with a fine resolution, over all important length scales, so that good overlaps are more likely to be achieved.

With blocking, the matrices live on ‘superlinks’ joining sites that are  $2^b$  lattice spacing apart, where  $b$  is the number of blocking iterations. Each iteration involves adding the direct path to 4 elongated staples,

$$\begin{aligned}\tilde{U}_i^{b+1}(n) &= U_i^b(n)U_i^b(n+2^b\hat{i}) \\ &+ p_a \sum_{j \neq i} U_j^b(n)U_i^b(n+2^b\hat{j})U_i^b(n+2^b\hat{j}+2^b\hat{i})U_j^{b\dagger}(n+2^{b+1}\hat{i}) \\ &+ p_a \sum_{j \neq i} U_j^{b\dagger}(n-2^b\hat{j})U_i^b(n-2^b\hat{j})U_i^b(n-2^b\hat{j}+2^b\hat{i})U_j^b(n-2^b\hat{j}+2^{b+1}\hat{i}),\end{aligned}\quad (20)$$

$$U_i^{b=0}(n) = U_i(n) \quad (21)$$

where again one projects  $\tilde{U}_i^{b+1}(n)$  into  $SU(N)$ ,

$$U_i^{b+1}(n) = \mathcal{U}\{\tilde{U}_i^{b+1}(n)\}, \quad (22)$$

and we form wavefunctions by multiplying these matrices around closed loops of the corresponding superlinks. Here one typically chooses  $p_a = O(1)$  so that the width of the blocked link increases at least in step with its length.

Blocking is faster because one smoothenes by a factor of two in size at each step. On the other hand the same factor of two gives it a rather crude resolution. If the size of the wavefunctional of the state of interest falls between two blocking levels then the overlap might well be suppressed leading to a poorer calculation than with a fine-grained smearing.

An obvious way to try and improve the above smearing is to make it more symmetric about the axis of the link. In eqn(17) we add to the link just the four nearest parallel links going outwards along the lattice axes. (The staples are just these link matrices parallel transported to the link of interest.) After a number of successive smearings this can lead to an operator with peculiar and unnatural axial rotation properties. A first step to alleviate this is to include the next set of parallel links, those which are a distance  $\sqrt{2}a$  away, diagonally across the square lattice. To parallel transport these requires a minimum product of 2 link matrices at each end, giving the algorithm

$$\begin{aligned}\tilde{U}_i^{s+1}(n) &= U_i^s(n) + p_a \sum_{j \neq i} U_j^s(n)U_i^s(n+\hat{j})U_j^{s\dagger}(n+\hat{i}) \\ &+ p_a \sum_{j \neq i} U_j^{s\dagger}(n-\hat{j})U_i^s(n-\hat{j})U_j^s(n-\hat{j}+\hat{i}) \\ &+ p_d \sum_{j \neq i} \sum_{k \neq i,j} U_j^s(n)U_k^s(n+\hat{j})U_i^s(n+\hat{j}+\hat{k}) \sum_{j' \neq i} \sum_{k' \neq i,j'} U_{j'}^{s\dagger}(n+\hat{i}+\hat{k}')U_{k'}^{s\dagger}(n+\hat{i}) \\ &+ p_d \{\text{rotations}\}\end{aligned}\quad (23)$$

with  $\tilde{U}_i^{s+1}(n)$  then being unitarised to  $U_i^{s+1}(n)$ . The term labelled ‘rotations’ refers to three further terms like the previous one, but rotated by a multiple of  $\pi/2$  around the  $i$ -axis (so that either  $j$  or  $k$  or both go backwards). So now the smearing consists of the direct path, the 4 staples and 16 ‘wiggly’ staples. We now have two parameters,  $p_a$  and  $p_d$ , to choose (see below).

As for blocking, an obvious variant of the algorithm in eqn(21), which is both more elegant and probably better (because it includes more paths), is to simply multiply two smeared links together

$$\begin{aligned} U_i^{b=1}(n) &= U_i^s(n)U_i^s(n + \hat{i}), \\ U_i^{b=1,s}(n) &= \mathcal{S}^s\{U_i^{b=1}(n)\}, \\ U_i^{b+1}(n) &= U_i^{b,s}(n)U_i^{b,s}(n + 2^b\hat{i}). \end{aligned} \tag{24}$$

Here  $U^s$  is a link that has been smeared  $s$  times, and  $\mathcal{S}$  denotes the smearing operation generalised to apply to blocked links. That is to say, in eqn(17) or eqn(23) the matrices are replaced by blocked matrices and the links are replaced by the appropriate superlinks. While each step of the old blocking iteration summed just 5 paths (at the previous blocking level) this improved blocking (using improved smearing) will sum  $21^2$  paths (ignoring double counting and cancellations) and will be more axially symmetric (with an appropriate choice of  $p_a, p_d$ ).

Clearly these algorithms can be applied in various combinations. We focus on three simple strategies.

- A) Iterated smearing using eqn(23) with small values of the parameters designed to give operators spanning all relevant scales with a fine resolution.
- B) Iterated blocking using eqn(24) and eqn(23) with larger values of the parameters, designed to rapidly go from ultraviolet to physical length scales.
- C) A hybrid where one initially blocks as in (B) and then multiply smears the blocked links as in (A). The (iterated) blocking is designed to rapidly take us to the lower limit of physically interesting length scales, with the subsequent smearing providing a fine-resolution exploration of the larger length scales.

To determine the best choice of parameters we will calculate the desired correlator and find which parameters give the best overlap onto the desired state.

#### 4.1.1 unitarisation

Before that, some comments. There is no fundamental reason why the smeared or blocked matrices should be unitary. However in practice one finds that projecting back to  $SU(N)$  produces eventual overlaps that are as good as with any other normalisation (and better than most). Thus it is convenient to unitarise. We unitarise by finding the  $SU(N)$  matrix  $U^b$  that maximises

$$\max_{U^b \in SU(N)} \text{ReTr}\{\tilde{U}^{b\dagger}U^b\} \tag{25}$$

and similarly for smearing. This can be done by using the  $\beta = \infty$  limit of the Cabibbo-Marinari heat bath, just as one does when ‘cooling’ lattice fields to calculate their topological

charge [19]. This is an iterative procedure which needs to start with some initial value for  $U^b$ , call it  $U_s^b$ . Typically one will choose  $U_s^b$  to be some very crude unitarisation of  $\tilde{U}^b$ . After one or two iterations one obtains a good approximation to  $U^b$  in eqn(25). The fact that this is an approximation means that one does not maintain exact gauge invariance. However all this will do is to increase slightly the statistical noise in the calculation of correlators. A second potential problem arises in the choice of the crude starting point,  $U_s^b$ . Typically this will not be the same for  $U^b$  and for  $U^{b\dagger}$ . For example if one obtains  $U_s^b$  by orthonormalising the columns of  $\tilde{U}^b$  one by one, as we do, one gets a different matrix than if one started by orthonormalising the rows. This effectively breaks the rotational symmetry and can undermine in a subtle way the assignment of  $J^{PC}$  quantum numbers in the construction of glueball operators <sup>2</sup>. In practice after the one or two cooling iterations that we normally perform in our calculations, the resulting matrix loses almost all memory of the starting matrix and the symmetry breaking is insignificant. If one needed to be more careful a simple remedy would be to choose to orthogonalise rows or columns at random, so that the symmetry would be restored in the ensemble.

## 4.2 numerical tests

The improved blocking we shall focus upon performs the blocking by multiplying together two once-smearred links as in eqn(24).

We illustrate the potential of operator improvement in Fig.1. Here we plot the effective mass versus  $n_t$  of the  $k = 2$  string that winds around the spatial torus, from a calculation [1] on a  $16^4$  lattice at  $\beta = 11.10$  in SU(4) using ‘old’ blocking for the (super)link construction. Loops are composed of (super)links that have been blocked up to four times, i.e. five blocking levels when we include no blocking at all. The linear combination of these five operators which minimises  $am_{eff}(t = a)$  is chosen as the best operator, and from its correlator we obtain  $am_{eff}(t = n_t a)$  in Fig.1. Note that this corresponds to a variational calculation of the ground state, where one maximises  $\exp -aH$  in this basis of five operators. We do the same with our improved blocking, with  $p_a = 0.40$  and  $p_d = 0.16$ , again on a  $16^4$  lattice for SU(4) and at the nearly identical coupling  $\beta = 11.085$ . We contrast the two calculations in Fig.1 where we see a dramatic improvement in the use of the new blocking technique: with the same statistics the errors on the final mass estimate are reduced by about a factor of two.

Clearly we need to determine the range of smearing/blocking parameters that provide the best improvement and also how many smearing or blocking steps need to be taken. To do this we perform calculations with a variety of different values of the parameters. Ideally we should calculate the overlaps onto the lightest states in the various channels of interest, so as to find the parameters that maximise these overlaps, i.e. the  $|c_n|^2$  in eqn(1). However usually we do not have enough accuracy to do this, and instead we calculate the effective mass from

---

<sup>2</sup>We are grateful to Harvey Meyer for pointing out to us this potential flaw in the usual blocking/smearing algorithms.

the values of the correlation function at  $t = 0$  and  $t = a$ :

$$am_{eff}(t = a) = -\ln \frac{C(t = a)}{C(t = 0)}. \quad (26)$$

Because of the positivity of our correlation functions, the lower the value of  $am_{eff}(a)$  the better, in a variational sense, is the operator.

We have performed a wide variety of tests and comparisons. For the sake of brevity we will choose to discuss only a subset of these here.

#### 4.2.1 blocking with smearing

In this calculation we perform multiple smearing upon blocked (super)links with  $(p_a, p_d) = (0.10, 0.0)$ . We block up to three times, with the ‘old’ blocking of eqn(21) with  $p_a = 1.0$ . The calculation is in SU(3) on a  $12^4$  lattice at  $\beta = 5.90$ . The purpose of this calculation is to see how many smearing and blocking steps one needs to perform for a useful improvement.

In Table 2 we show the values of  $am_{eff}(t = a)$  for the  $0^{++}$  glueball operator based on  $1 \times 1$  loops (‘superplaquettes’) made out of superlinks that have been blocked  $b = 0, \dots, 3$  times and then smeared up to 14 times. We see that if one blocks too few times then one needs a large number of smearing steps to obtain a useful improvement while if one blocks too many times the operators are worse and cannot be improved by subsequent smearing. In this particular case the most efficient strategy appears to be to block twice and then to smear about four times. If one smears too many times, again the overlap gets worse.

For comparison we also show what one gets with the improved blocking with parameters  $(p_a, p_d) = (0.40, 0.16)$ . Although it appears that we could obtain a further small improvement in the overlap with further multiple smearings, we shall not explore this possibility here and shall from now on focus on simple improved blocking.

#### 4.2.2 improved blocking

In this calculation we perform improved blocking with various values of  $(p_a, p_d)$  on a  $12^4$  lattice at  $\beta = 10.90$  in SU(4). We perform  $b = 0, 1, 2, 3$  blockings and use the various blocking levels to construct our operators. So for each state we have a basis of operators and within this basis we find the linear combination that minimises  $am_{eff}(t = a)$ . So  $am_{eff}(t = a)$  is our best variational estimate of the mass of the ground state in the channel of interest.

The channels we focus upon are the fundamental (i.e.  $k=1$ ) string with  $\vec{p} = 0$ , the same string with the lowest non-zero momentum, i.e.  $a\vec{p} = 2\pi/L_s$ , the  $k = 2$  string and the lightest scalar and tensor glueballs.

In Table 3 we list the values of  $am_{eff}(t = a)$  that we obtain for the values of  $p_a, p_d$  shown. We see that although the best values of the parameters differ for different states, in practice values like  $(p_a, p_d) = (0.30, 0.12)$  or  $(p_a, p_d) = (0.40, 0.16)$  are a good compromise giving close to the best overlaps for all the states. These are therefore the values we shall use in the rest of this paper.

The calculations we shall describe later on in this paper are with high enough statistics that one can extract the overlap onto the lightest state quite accurately. One can do the same

for the calculations in [1, 2] and so compare the overlaps one obtains with ‘old’ and improved blocking. This we do in Table 4 for the lightest  $k = 1$  and  $k = 2$  strings and the lightest scalar glueball, for our various SU(4) calculations. We observe a very large improvement in all cases with our new techniques, particularly for the  $k = 2$  string.

## 5 Some results

To calculate the lightest mass in a given sector of string or glueball states, we perform a standard variational calculation with different blocking and/or smearing levels, and sometimes different loops, providing the basis of operators.

In Tables 5 to 9 we list the masses of the lightest and first excited  $0^{++}$  glueballs, the mass of the lightest  $2^{++}$  glueball, and the tension of the fundamental ( $k = 1$ ) string. Tables 10 and 11 contain our values of the tensions of  $k \geq 2$  strings. All these calculations use improved blocking, as in eqn(23) and eqn(24), with  $(p_a, p_d) = (0.30, 0.12)$  or  $(0.40, 0.16)$ .

The results of our SU(4) anisotropic lattice calculations are listed in Tables 12 and 13. Here we use one or two blockings plus multiple smearing but, because these were earlier calculations, the smearing was of the old variety, as in eqn(17). The bare anisotropy we chose was  $\xi = 0.5$  but, as we see from Table 13, the renormalised anisotropy (determined as described in Section 2) is smaller by  $\sim 8\%$  and, as expected,  $\xi_r \rightarrow \xi$  as  $a \rightarrow 0$ . Comparing the values of  $a_s\sigma = a_t\sigma/\xi_r$  from Table 13 to the values in Table 7, we see that the tree level value of  $\beta$ , as in eqn(9), is also significantly renormalised. For example our anisotropic calculation at  $\beta = 11.325$  has  $a_s\sqrt{\sigma}$  nearly identical to that at  $\beta = 11.085$  in the isotropic calculation.

We can use the fact that the isotropic  $\beta = 11.085$  and anisotropic  $\beta = 11.325$  calculations have essentially the same  $a_s$  and spatial size,  $a_s L_s = 16a_s$ , and very similar statistics, to compare directly the corresponding correlation functions. This we do in Fig.2 for the lightest  $k = 2$  periodic flux loop. We plot the effective mass, as defined in eqn(13), against  $n_t$ . In the case of the isotropic calculation we scale  $n_t$  up by a factor of  $1/\xi_r$  (although we leave the mass expressed in units of the original lattice spacing, so that its value is about a factor of  $1/\xi_r$  larger). We also show the final mass estimates which we obtain using exponential fits to the correlation functions. We see that although the  $a_t$  we use only differs by a little more than a factor of two between the two calculations, the extra resolution in  $t$  provides us with much more convincing evidence for an effective mass plateau. This demonstrates the utility of such anisotropic calculations.

The SU(8) calculations possess about half the statistics of the other calculations, and the errors are probably underestimated. In particular the mass estimates of heavier states, such as strings of larger  $k$ , will suffer from the systematic errors spelt out earlier.

### 5.1 glueballs

We extrapolate to the continuum limit with an  $O(a^2)$  correction:

$$\frac{m_G}{\sqrt{\sigma}}(a) = \frac{m_G}{\sqrt{\sigma}}(0) + ca^2\sigma. \quad (27)$$

The results are listed in Table 14. These continuum mass ratios can now be extrapolated to  $N = \infty$  with an  $O(1/N^2)$  correction:

$$\frac{m_G}{\sqrt{\sigma}}(N) = \frac{m_G}{\sqrt{\sigma}}(\infty) + \frac{c}{N^2}. \quad (28)$$

This is shown in Fig.3 and the  $N = \infty$  limits are listed in Table 14.

We make several observations. First, our  $N = \infty$  mass ratios are compatible with previous results [2] but the errors have been reduced by about a factor of two. The individual  $SU(N)$  continuum limits of the two heavier states are typically lower by about one standard deviation however, and we put this down to the reduction in systematic errors arising from our improved operators. The  $0^{++}$  has a scatter which may arise from the finite volume effects discussed earlier. Nonetheless, we see that its mass is roughly twice that of the lightest scalar. Finally we observe in Fig.3 that with these more accurate calculations, it has become impossible to include the  $SU(2)$  value of the  $2^{++}$ , and perhaps the  $0^{++}$ , in a fit including just the leading  $O(1/N^2)$  correction.

Our continuum extrapolations only involve a few lattice spacings and one might worry that this may give the coarser lattice spacings too much influence. It is therefore interesting to compare the mass ratios calculated on the smallest value of  $a$  that is ‘common’ to all  $N$ . In practice we mean by this that  $a\sqrt{\sigma} \in [0.195, 0.210]$  for all  $N$  except for  $SU(2)$  where  $a\sqrt{\sigma} \simeq 0.24$ . This  $a$  is well in the scaling regime where lattice corrections are small. All calculations are on  $16^4$  lattices. We list the mass ratios in Table 15 and plot them against  $1/N^2$  in Fig.4, where we show large- $N$  extrapolations of the form in eqn(28). The errors are smaller than for the continuum extrapolations, and it is now clear that none of the  $SU(2)$  masses fall onto such a simple fit. It is interesting that the  $0^{++}$  is much better behaved than in Fig.3 and that at this (small) value of  $a$  it is very close to twice the mass gap.

## 5.2 k-strings

The string tensions for  $N = 4, 6, 8$  are listed in Tables 10 and 11. The ratio of the  $k = 2$  string tension to  $\sigma$  is plotted against  $a_s^2\sigma$  in Fig.5 for both the isotropic and the anisotropic  $SU(4)$  lattice calculations. In the anisotropic calculation we take advantage of the extended, finer resolution in  $t$  to use exponential fit ranges that are roughly constant in physical units. In this way we hope to minimise the systematic errors discussed earlier, albeit at the price of somewhat larger statistical errors. We show continuum fits of the form in eqn(27). In Fig.6 we do the same for the  $k = 2, 3$  strings in  $SU(6)$ , and in Fig.7 for the  $k = 2, 3, 4$  strings in  $SU(8)$ , all on isotropic lattices. The higher- $k$   $SU(8)$  calculations, which are simultaneously more massive and are performed with half the statistics of other calculations, no doubt suffer rather severely from the systematic errors we emphasised earlier, as suggested by the apparent increase in the ratio with decreasing  $a$ .

Our continuum limits of  $\sigma_k/\sigma$  are listed in Table 16 and compared with the values suggested by ‘Casimir Scaling’ and ‘MQCD’. We see that our values fall between these two sets of predictions, except for the  $k = 3, 4$   $SU(8)$  calculations – but these we discount, because they are by far the poorest.

It is interesting to see by how much our calculation of  $\sigma_k$  improves upon previous calculations. In Fig.8 we plot the SU(4) values of  $a^2\sigma$  and  $a^2\sigma_{k=2}$  as obtained in the present calculation and in that of [1]. We observe that our values are slightly lower with the difference larger for  $k = 2$  than for  $k = 1$  – precisely as we would expect from the systematic error described earlier. Because of the positivity of our correlators, if the extracted mass is lower then the calculation is unambiguously better. In Fig.9 we compare our SU(6) calculations with those of [10]. Here the masses are even heavier and the improvement much more marked. Although our statistics is an order of magnitude less than that of [10] our better operators clearly provide an unambiguously better calculation.

## 5.3 unstable strings

### 5.3.1 background

At finite  $N$  the only strings that are absolutely stable are the  $k$ -strings. However for each value of  $k$  there are sources in many representations, and for each such source there will be a string (or strings) carrying its flux. At finite  $N$  such strings can be screened by the gluons in the vacuum, down to the lightest string of the same value of  $k$ . However this charge screening/string breaking typically vanishes as  $N \rightarrow \infty$ , so that the string become increasingly stable and well-defined in that limit.

Typically the source arises from a direct product of  $k + j$  fundamental and  $j$  conjugate fundamental sources. Thus if screening is suppressed one would expect that over long enough distances the flux will travel through  $k + 2j$  fundamental flux tubes, i.e.

$$\sigma_{k+j,j} = (k + 2j)\sigma \tag{29}$$

unless these strings form a bound state of lower tension. Of course it is only for  $N \rightarrow \infty$  that screening can be neglected for arbitrary separations, and in that limit we expect string binding to vanish, so that the string that becomes stable has a tension that is precisely  $(k + 2j)\sigma$ . The classic example of this is the  $k = 0$  adjoint string, where we expect  $\lim_{N \rightarrow \infty} \sigma_A = 2\sigma$ . What would be interesting is not so much the verification of eqn(29), but the observation of a bound state or resonant string at finite  $N$ . Of course, since the large- $N$  counting tells us to expect the binding to be of the order of the decay width (per unit length), it is not at all obvious that there is anything unambiguous to find.

Recent calculations of the tension of the adjoint string and of several other unstable strings in SU(3) [20, 21] have turned out to be consistent with Casimir Scaling. That is to say, they typically find string tensions that are larger than in eqn(29). These calculations have been performed with explicit sources (i.e. using Wilson rather than Polyakov loops) and have exploited the fact that in such a set-up any flux tube will remain completely stable up to some finite distance. This distance is determined by the trade-off between the extra mass the source acquires if it is to be screened, and the decrease in the string energy induced by the screening. In practice the distance between the sources for which the potential energy can be calculated is limited to about 1fm, and some fraction of this distance falls into the Coulomb region around the sources – so that the actual strings are probably no more than  $\sim 0.5$ fm in length. This is

too short a length for us to be entirely confident that we are seeing the asymptotic string-like properties of the flux tube, and in particular where we would expect eqn(29) to give a lighter state of this system. Moreover, since the Coulomb interaction that dominates the potential at shorter distances trivially satisfies Casimir Scaling, one might worry that what we are seeing at separations  $\leq 1\text{fm}$  is some subasymptotic dynamics that manifests approximate Casimir Scaling by continuity with one gluon exchange. Alternatively it might be a genuine resonant multi-string state, whose break-up into the separate fundamental strings requires tunnelling through some barrier.

It would clearly be interesting to investigate such unstable strings using the formalism where the string winds around the torus so that there are no sources, and there is no Coulomb piece with Casimir Scaling. Moreover, in our typical calculation the length of the string is  $a_s L_s \sim 3.2 \sim 1.5\text{fm}$ , if we introduce ‘fm’ units through  $\sqrt{\sigma} \simeq 0.45\text{fm}$  (the value in QCD). This is long enough that it might be asymptotic. The downside is that there is no length below which such an unstable string will be stable; its approximate stability will depend entirely on  $N$  being large enough, and we do not know in advance what that will be.

We will focus here on the totally symmetric and antisymmetric  $k = 2$  and  $k = 3$  strings, and in addition the mixed  $k = 3$  string, which we refer to as  $kS, kA$  and  $kM$  respectively. (See Appendix A of [1] for the details of the operator construction.) We recall that in similar calculations in [1] there was no good evidence found for such strings in  $D = 3 + 1$   $SU(N)$  gauge theories, although some evidence was found in the case of  $D = 2 + 1$ . This might be because in [1] the operators for strings of higher  $k$  were much poorer in  $D = 3 + 1$  than in  $D = 2 + 1$ . With the improved operators of the present paper we can hope to do better.

In this Section we will compare our results to Casimir Scaling not so much because the theoretical case is at all compelling, but rather because there is at least a formula to compare with – unlike the case of ‘MQCD’ which (as far as we know) makes no predictions for such unstable strings. It may be useful to reproduce the expressions relevant to our calculations:

$$\frac{\sigma_k}{\sigma} \stackrel{CS}{=} \begin{cases} k(N - k)/(N - 1) & : \text{ anti-symmetric} \\ k(N + k)/(N + 1) & : \text{ symmetric} \\ 3(N^2 - 3)/(N^2 - 1) & : \text{ k=3, mixed.} \end{cases} \quad (30)$$

(See Appendix A of [1] for the derivation.)

### 5.3.2 results

We will begin with our results from the calculation on the  $SU(4)$  anisotropic lattice with the smallest  $a_s$  and  $a_t$ , i.e. the  $16^3 40$  lattice. We would hope that the fine resolution in  $t$  will provide us with our best chance of seeing some kind of effective mass plateau (albeit temporary in  $t$ ) for the heavy unstable string of interest. On the other hand  $N = 4$  might be too small for these strings to be sufficiently stable and well defined.

In Fig.10 we show the effective mass as a function of  $n_t$  for the lightest  $k = 1$ ,  $k = 2A$  and  $k = 2S$  string states, as obtained from a variational calculation [1] using the basis of multiply-smearred blocked Polyakov loop operators described at the beginning of this Section.

Some observations:

- The lightest  $k = 2$  string is in the totally antisymmetric representation,  $2A$ . This is true for all our  $k$  and  $N$  (and was already noted in [1]).
- The lightest string in the  $2S$  representation appears to be much heavier, and we have significant evidence for an effective mass plateau.
- The apparent absence of the lightest  $2A$  state in the mass spectrum obtained with the  $2S$  operators, tells us that the overlap of this state onto this basis must be very small; at most at the percent level. This is presumably the expected large- $N$  suppression and suggests that for the present purposes  $N = 4$  is ‘large’.
- We show in Fig.10 the masses we would obtain for the  $k = 2A$  and  $k = 2S$  strings if we assumed Casimir Scaling, and scaled up from the  $k = 1$  mass using eqn(14) and eqn(30). We see that Casimir Scaling works quite well here.

On our isotropic lattices we cannot hope to go to large enough  $n_t$  to obtain serious evidence for any effective mass plateaux for these heavy strings. We will assume on the basis of our above anisotropic lattice calculation that these approximate plateaux do exist. We will not attempt continuum extrapolations, for obvious reasons, but will simply work at the smallest  $a$  at each  $N$  i.e. on the  $16^4$  lattices for  $N = 4, 6, 8$ . We will typically extract the mass from  $t = a$  to  $t = 2a$ . (We note that this corresponds to  $m_{eff}(n_t \geq 3)$  in our anisotropic lattice calculation, and we see from Fig.10 that such masses already lie, more-or-less, on the corresponding plateaux.) In Table 17 we list the lightest  $2A, S$  masses for  $N = 4, 6, 8$  and the lightest  $3A, S, M$  masses for  $N = 6, 8$ . We also list the masses one would expect from Casimir Scaling (scaled up from the  $k = 1$  masses using eqn(14)). Overall we find qualitative compatibility with the Casimir Scaling formula in eqn(30), and also some sign that the agreement improves as  $N$  increases. However there are a number of other features of the spectrum that are both interesting and puzzling, and which need to be understood before the comparison in Table 17 can be taken too seriously.

### 5.3.3 puzzles

The main puzzle is an unexpected (to us) pattern of degeneracies. A striking illustration is provided in Fig.11, where we plot  $am_{eff}(n_t)$  for the first excited state of the  $2A$  string and compare it to the ground state of the  $2S$  string (as plotted in Fig.10). We see that the two states are, within errors, degenerate with each other. Although this degeneracy is most convincing on an anisotropic lattice, because of the finer resolution in  $t$ , we see good evidence for similar degeneracies on the isotropic lattice calculations, as shown in Table 18. Interestingly we see there some evidence that the near-degeneracy becomes less precise with increasing  $N$ . When we look at the  $k = 3$  strings we observe analogous degeneracies. We observe in Tables 19 and 20 that the first excited  $3A$  string has a similar mass to the ground state  $3M$  string, and that the first excited  $3M$  and, more approximately, the second excited  $3A$ , have the same mass as the lightest  $3S$  string. In all these cases these are real near-degeneracies – they are not the same states appearing from variational analyses using different but overlapping sets of operators. We can verify this (see below) by performing variational calculations with the full basis of  $k = 2$  or  $k = 3$  operators, whereupon we find these near-degenerate states appearing

there as separate states, with approximately the same masses.

These near-degeneracies are, of course, only significant to the extent that the energy differences are much less than typical splittings between excited states. To demonstrate this in the case of SU(4) we list in Table 21 the values of  $am_{eff}(t = a)$  for the string ground state and the next few excited states. We do so for the  $k = 1$ ,  $k = 2$  and for the  $k = 2A, S$  representations, for both the anisotropic and isotropic lattice calculations with the smallest values of  $a$ . Of course  $am_{eff}(a)$  is not ideal; it would be better to use  $am_{eff}(t)$  at a larger value of  $t$ . However in the case of the highly excited states, values of  $am_{eff}(t > a)$  are too imprecise to be useful. So to keep the treatment uniform we use this measure of the energy for all states. Note that our variational calculation is based on maximising  $\exp -aH$ , so  $am_{eff}(a)$  is precisely the mass estimate provided by the variational calculation. One first calculates the ground state using all operators, then the first excited state in the basis orthogonal to this ground state, and so on. This means that the higher excited states are determined using an ever-smaller basis, and are less reliable. In practice our  $k = 1$ ,  $k = 2A, S$  and  $k = 3A, S, M$  bases contain 5 or 10 operators each for the isotropic and anisotropic calculations respectively, while the  $k = 2, 3$  bases are 2 or 3 times as large.

Focussing first on the anisotropic lattice calculation, we see in Table 21 that there is an extensive pattern of near-degeneracies

$$m_{2S} \simeq m_{2A}^* \quad ; \quad m_{2S}^* \simeq m_{2A}^{**} \quad ; \quad m_{2S}^{**} \simeq m_{2A}^{***} \quad ; \quad \dots \quad (31)$$

These states appear as separate states in the  $k = 2$  spectrum (also shown). Other than these near-degeneracies, the typical splittings in the  $k = 1$ ,  $k = 2A, 2S$  and  $k = 3A, 3S, 3M$  spectra, are very much larger,  $a_t \Delta E \sim 0.4$ , justifying our use of the term ‘nearly degenerate’. We also note some evidence that the degeneracy becomes less exact for the higher excitations. Finally we note that the same pattern appears in the isotropic lattice calculation.

Analogous results for  $k = 2$  and  $k = 3$  strings in SU(6) and SU(8) are listed in Table 22 and Table 23. In the  $k = 2$  sector we only have a clear near-degeneracy between  $m_{2S}$  and  $m_{2A}^*$  and even that is weaker than for SU(4). In the  $k = 3$  sector we note

$$m_{3M} \simeq m_{3A}^* \quad ; \quad m_{3S} \simeq m_{3M}^* \sim m_{3A}^{**} \quad (32)$$

with the relation denoted by ‘ $\sim$ ’ being less certain. Indeed in SU(8) the evidence is more for  $m_{3S}^* \sim m_{3A}^{**}$ .

It is interesting to ask what happens in SU(2) and SU(3). Unfortunately in most of those calculations we did not include  $k > 1$  strings (for obvious reasons) and we cannot present results at the same  $a$  and on the same volume as for  $N \geq 4$ . Instead we show an example for each of  $N = 2$  and  $N = 3$  in Table 24. In SU(2) the  $k = 2A$  operator is just a constant and this also renders the  $k = 2$  diagonalisation singular. In the  $k = 2S$  sector we see non-trivial masses, although the effective mass plateaux are often not well defined. We note that the lightest  $k = 2S$  state is significantly below the Casimir Scaling prediction. In the case of SU(3) two fundamental fluxes can become a single (conjugate) fundamental flux and we see this in the fact that the  $k = 1$  loop mass appears as the lightest  $k = 2A$  (and  $k = 2$ ) state. This is also what one expects from Casimir Scaling. We also see that just as in SU( $N \geq 4$ ) the

lightest  $k = 2S$  state is nearly degenerate with the first excited  $k = 2A$ . Both states appear in the  $k = 2$  spectrum showing that they are indeed different states. An extra oddity in SU(3) is that the first excited  $k = 1$  state has the same mass. We might expect it to appear in the  $k = 2A$  spectrum just as the lightest  $k = 1$  state does. On the other hand we have the same  $k = 2S, 2A^*$  near-degeneracy in SU(4) where we do not expect the  $k = 1$  states to appear in the  $k = 2$  spectrum. Despite this, in SU(4) the first excited  $k = 1$  state does indeed have a mass that is not very different from that of these  $k = 2$  states. All this accentuates the puzzle of these spectra.

As a first step towards understanding these apparent near-degeneracies, it might help to consider what kind of ‘excited’ states we might expect to find.

- The  $k = 2(3)$  operators should project onto scattering states of two (three)  $k = 1$  loops. Where will such states lie? We observe that the relevant  $k = 2$  operator is a product of two  $k = 1$  lines at the same position; thus it projects onto all relative momenta. (The total momentum being zero of course.) On a  $L_s = 16$  lattice one can estimate that the correlator of an operator that projects equally onto all lattice momenta will lead to  $m_{eff}^{k=2}(a) \sim 3$  with the precise value depending on the lattice corrections to the energy-momentum dispersion relation. Thus the scattering states should appear at the upper end of the mass range we are considering. On the other hand because the string operators are highly smeared in the directions transverse to the string axis, one might expect the overlap onto higher momenta to be suppressed. If this suppression were quite radical then it might be that the spectra we are seeing could be related to the lightest 2 or 3 string scattering states (including excitations of the latter). To resolve this issue definitively one would need to include explicit scattering state operators in the basis and examine overlaps. These states would need to include a large range of relative momenta as well as excitations of the  $k = 1$  strings. Such a calculation goes well beyond what we are attempting here.
- In our basis we do not include the conjugate operators which, if we did, would lead to trivial degeneracies (even in the  $k = 1$  sector). However in SU(4) the  $k = 2$  and conjugate,  $k = -2$ , operators ‘mix’ because  $z^2 = z^{*2}$ ,  $\forall z \in Z_4$ . Thus all  $k = 2$  excitations might form  $C = +$  and  $C = -$  linear combinations leading to an approximate doubling in the  $k = 2$  spectrum. This might be a factor in the more extensive degeneracy structure that we see in SU(4). (The same argument would apply to  $k = 3$  in SU(6).) On the other hand it should also apply to the lightest  $k = 2A$  state for which there is no degeneracy. So this seems unlikely.
- We note that our operators are maximally symmetric, not only so as to have  $\vec{p} = 0$ , but also with respect to translations along the axis of the loop and rotations around the axis. Nonetheless since we only have lattice symmetries, somewhere amongst the excited states of the strings will be states that in the continuum become states with spin  $J = 4$  around the string axis. In a simple string model, the pattern of fluctuations of  $J \neq 0$  and excited  $J = 0$  states is related and perhaps leads to some of the degeneracy structure. This is also something to consider.
- There will also be states involving compression waves along the flux tube, but we have no idea of the mass scale of these.

None of the above provides an immediate explanation for the pattern of degeneracies we observe. This makes our study of the unstable strings much more ambiguous than that of the

stable strings.

## 6 Mass calculations in the $N \rightarrow \infty$ limit

We expect correlators of gauge invariant operators to factorise at large  $N$ , e.g.

$$\langle \Phi^\dagger(t)\Phi(0) \rangle \stackrel{N \rightarrow \infty}{\equiv} |\langle \Phi \rangle|^2 \{1 + O(\frac{1}{N^2})\} \quad (33)$$

where  $\Phi$  is some typical glueball or string single-trace trial wavenfunctional. This means that the connected piece of the correlator, from which we extract masses, should vanish rapidly at large  $N$ :

$$\sum_{n \neq \Omega} |\langle \Omega | \Phi^\dagger | n \rangle|^2 e^{-E_n t} \stackrel{N \rightarrow \infty}{\equiv} O(\frac{1}{N^2}) \times |\langle \Omega | \Phi^\dagger | \Omega \rangle|^2 \quad (34)$$

where  $|\Omega\rangle$  is the vacuum state. If this is really so, does it mean that mass calculations become increasingly difficult as  $N \rightarrow \infty$ ?

To see if the factorisation in eqn(33) does indeed occur in the range of  $N$  that we study, we calculate the correlation function

$$C_2(t) = \frac{\langle \Phi(t)\Phi(0) \rangle}{\langle \Phi \rangle^2} - 1 = \frac{\langle \Phi_v(t)\Phi_v(0) \rangle}{\langle \Phi \rangle^2} \quad (35)$$

where

$$\Phi_v(t) = \Phi(t) - \langle \Phi \rangle \quad (36)$$

and  $\Phi$  is the thrice-blocked (super-)plaquette  $0^{++}$  glueball operator (which is real so we drop the conjugation from now on).  $C_2(t)$  is the vacuum subtracted correlator normalised by the disconnected piece and, if calculated at fixed  $a$ , it should be  $\propto 1/N^2$  as  $N \rightarrow \infty$ . We use our calculations on  $10^4$  lattices at  $a \simeq 1/5T_c$ , all of which use  $10^5$  Monte Carlo sweeps for the averages. Thus the calculations are as nearly identical as possible, apart from the variation with  $N$ . (We have checked that if one fixes  $a$  using the string tension rather than  $T_c$  it makes no difference to our conclusions.) We note that at this value of  $a$  the above operator has a very large overlap onto the lightest scalar glueball.

We plot the values of  $C_2(t=0)$  multiplied by  $N^2$  in Fig.12. We see that for  $N \geq 3$  we obtain a good fit to the form

$$N^2 C_2(t=0) = 2.751(10) - \frac{4.11(17)}{N^2}. \quad (37)$$

This demonstrates that the correlators we use for our mass calculations do indeed show the expected suppression with increasing  $N$ , even at the smallest values of  $N$ . That is to say our ‘measured signal’ – the connected piece of the two-point correlator when normalised to the disconnected piece – does indeed vanish rapidly with increasing  $N$ .

How does all this affect the accuracy of our mass calculations? This will be determined by how the fluctuations of  $C_2(t=0)$  vary with  $N$ . We calculate these from

$$\begin{aligned}\sigma_c^2(t) &= \langle \{ \Phi_v(t)\Phi_v(0) - \langle \Phi_v(t)\Phi_v(0) \rangle \}^2 \rangle \\ &= \langle \Phi_v(t)\Phi_v(0)\Phi_v(t)\Phi_v(0) \rangle - \langle \Phi_v(t)\Phi_v(0) \rangle^2\end{aligned}\tag{38}$$

and the  $N$ -dependence of the fluctuations on the correlator  $C_2(t=0)$  will be given by

$$\sigma[C_2(t)] = \frac{\sigma_c(t)}{\langle \Phi \rangle^2}.\tag{39}$$

We plot the ratio of this quantity to  $C_2(t=0)$  in Fig.13. We see that this ratio becomes rapidly independent of  $N$  as  $N$  increases. That is to say, the fluctuations of the connected 2-point correlator decrease with  $N$  in the same way as the correlator itself and masses can, in principle, be extracted with more-or-less the same precision at all  $N$ .

What we observe numerically is in fact what one expects from the usual large- $N$  counting. The 4-point correlator in eqn(38) contains (despite first appearances)  $\langle \Phi_v\Phi_v \rangle \langle \Phi_v\Phi_v \rangle$  disconnected pieces which will dominate the correlator at large  $N$ . Thus  $\sigma_c(t)$  will have the same  $N$ -dependence as our connected two point correlator,  $\langle \Phi_v(t)\Phi_v(0) \rangle$ , and our above results are in accordance with this expectation.

As an aside we recall (rearranging the fields) that

$$\begin{aligned}\sigma_c^2(t) &= \langle \Phi_v(t)\Phi_v(t)\Phi_v(0)\Phi_v(0) \rangle - \langle \Phi_v(t)\Phi_v(0) \rangle^2 \\ &= \sum_n |\langle \Omega | \Phi_v\Phi_v | n \rangle|^2 e^{-E_n t} - \left\{ \sum_n |\langle \Omega | \Phi_v | n \rangle|^2 e^{-E_n t} \right\}^2 \\ &\stackrel{t \rightarrow \infty}{=} |\langle \Omega | \Phi_v\Phi_v | \Omega \rangle|^2.\end{aligned}\tag{40}$$

That is to say, the errors become independent of  $t$  at larger  $t$ , so that the error-to-signal ratio grows  $\propto \exp +mt$  if  $m$  is the mass we are trying to calculate. Moreover as  $N$  decreases this behaviour will set in at smaller  $t$  since the disconnected piece becomes increasingly dominant. As is well known, for hadrons that are not flavour singlets the correlator explicitly excludes such a disconnected piece, and the  $t$ -dependence of the error-to-signal ratio is much more favourable.

We have seen that the correlator and its fluctuations decrease in the same way with increasing  $N$  so that in principle the error on the ‘same’ Monte Carlo calculation can be the same at all  $N$ . Do our calculations achieve this ideal in practice? To answer this question we plot in Fig.14 the error-to-signal ratio on our connected 2-point correlator at both  $t=0$  and  $t=a$  as a function of  $N$ . Recall that the same number of lattice fields are used in each calculation. We observe that this ratio is independent of  $N$  up to fluctuations that are presumably within the error on the errors (which are not shown because they have not been calculated). Thus large- $N$  factorisation does not make mass calculations any more difficult.

## 7 Discussion

In this paper we introduced some improved algorithms for constructing operators with very good overlaps onto the physical states of  $SU(N)$  gauge theories. We performed a variety of tests and comparisons and identified a range of parameters that work well.

Using these techniques we performed calculations of the lightest glueballs and  $k$ -strings for  $N = 2, 3, 4, 6, 8$ . The glueball results are consistent with earlier work, although with improved accuracy and a greater lever arm in  $N$ . Our accuracy has improved sufficiently that we are beginning to find that the  $SU(2)$  masses cannot be described by just a  $1/N^2$  correction to  $N = \infty$ , even though the corrections are small. We confirm that  $SU(3) \simeq SU(\infty)$ .

The focus of our calculations was on  $k$ -string tensions. We emphasised the main systematic errors. The first simply arises from the fact that the mass of the string increases with  $k$  and the natural systematic bias is for its mass to be extracted at too small a value of  $t$  and so to be increasingly overestimated for larger  $k$  and larger  $N$ . The step we made towards solving this problem was to construct operators with very good overlaps onto the lightest  $k$ -strings. Comparing our results with earlier  $SU(4)$  and  $SU(6)$  calculations we saw that our calculations improved significantly upon that earlier work. (The criterion of ‘improvement’ is unambiguous because of the positivity of the lattice action.) In particular it is clear that the string tension ratios are below the predictions of ‘MQCD’. Our current calculations suggest that they are above ‘Casimir Scaling’ but it is possible that more precise calculations will alter this conclusion.

The main caveat on our  $k$ -string calculation concerns the leading string correction that we (and others) use. Previous work suggests that it is very accurate for spatial sizes  $l\sqrt{\sigma} \geq 3$ , but this has not been investigated with great accuracy for larger  $k$  (and  $N$ ). We showed that a natural physical picture suggested that this would be an increasing underestimate as  $N$  grows. This is an important source of potential systematic error which could, in principle, lift the ratios up to the ‘MQCD’ values. Although this seems unlikely for our range of  $N$ , this judgement is based on simple-minded estimates that might be incorrect. This is a problem that needs to be addressed.

We also attempted to find evidence for other, unstable, strings. Using a calculation with an anisotropic lattice,  $a_t \ll a_s$ , we found significant evidence for a string of this type. This calculation adds to previous work on this issue, in that our string winds around the torus and so is without the sources which might otherwise confuse the issue with their Coulomb interaction. We found in addition an intriguing pattern of near-degeneracies for which we could produce no simple explanation. All this needs to be better understood – in particular the role of multi-string scattering states – before one can claim support for one theoretical picture or another.

Although the ‘MQCD’ and ‘Casimir Scaling’ formulae have some theoretical motivation, they are also very interesting in that while the former has the conventional  $O(1/N^2)$  correction to the large- $N$  limit, Casimir Scaling has an unconventional  $O(1/N)$  correction. We recall that the argument for  $O(1/N^2)$  is from diagrams to all orders, and one might speculate that the result might be different for completely non-perturbative objects like strings. Whether this makes the question interesting (see e.g. [22]) or tells us that ‘Casimir Scaling’ is excluded

(see e.g. [23]) is controversial. In any case it is interesting to see if our calculation tells us something about the correction in a model-independent way. To investigate this we take our  $k = 2$  string results, which are reasonably accurate for all  $N$ , and we parameterise them as

$$2 - \frac{\sigma_k}{\sigma} = \frac{c}{N^\alpha}. \quad (41)$$

In Fig.15 we plot our results for this on a logarithmic plot, and we see that the best fits give

$$\alpha = \begin{cases} 1.82 \pm 0.35 & : N \geq 4 \\ 1.36 \pm 0.98 & : N \geq 6 \end{cases} \quad (42)$$

It is clear that to have something really useful on this question we require calculations that are an order of magnitude more precise.

Finally we asked whether the vanishing of fluctuations in the  $N = \infty$  limit presents an obstruction to the calculation of masses at large  $N$  – given that we calculate masses from the correlation between such fluctuations. We saw that the connected 2-point correlators we use for our mass calculations do in fact show the expected rapid suppression with increasing  $N$ , even at small  $N$ . However we also saw that the fluctuation of such a connected 2-point correlator about its average decreases with  $N$  in the same way, so that the ‘error-to-signal’ ratio is more-or-less independent of  $N$ . We conclude that correlators encode masses with much the same precision at all values of  $N$ , even if at  $N = \infty$  there are in fact no fluctuations to correlate.

## Acknowledgements

We have had useful conversations with many colleagues, including Adi Armoni, Chris Korthals-Altes and Harvey Meyer. Our lattice calculations were carried out on PPARC and EPSRC funded Alpha Compaq workstations in Oxford Theoretical Physics, and on a desktop funded by All Souls College. During the course of most of this research, UW was supported by a PPARC SPG fellowship, and BL by a EU Marie Skłodowska-Curie postdoctoral fellowship.

## References

- [1] B. Lucini and M. Teper, Phys. Rev. D64 (2001) 105019 (hep-lat/0107007).
- [2] B. Lucini and M. Teper, JHEP 0106 (2001) 050 (hep-lat/0103027).
- [3] M. Teper, Phys. Lett. B183 (1987) 345; B185 (1987) 121.
- [4] M. Albanese et al, Phys. Lett. B192 (1987) 163; B197 (1987) 400.
- [5] K. Ishikawa, G. Schierholz and M. Teper, Z. Phys. C19 (1983) 327.  
C. Morningstar and M. Peardon, Phys. Rev. D56 (1997) 4043 (hep-lat/9704011).

- [6] G. 't Hooft, Nucl. Phys. B72 (1974) 461.  
E. Witten, Nucl. Phys. B160 (1979) 57.  
S. Coleman, 1979 Erice Lectures.  
A. Manohar, 1997 Les Houches Lectures, hep-ph/9802419.  
S.R. Das, Rev. Mod. Phys. 59(1987)235.  
Y. Makeenko, hep-th/0001047.
- [7] G. 't Hooft, in *Large N QCD* (Ed. R.F. Lebed, World Scientific 2002)  
(hep-th/0204069).
- [8] M. Luscher, K. Symanzik and P. Weisz, Nucl. Phys. B173 (1980) 365.  
Ph. de Forcrand, G. Schierholz, H. Schneider and M. Teper, Phys. Lett. B160 (1985) 137.
- [9] M. Teper, Phys. Rev. D59 (1999) 014512 (hep-lat/9804008).
- [10] L. Del Debbio, H. Panagopoulos, P. Rossi and E. Vicari, JHEP 0201 (2002) 009  
(hep-th/0111090).
- [11] J. Ambjorn, P. Olesen and C. Peterson, Nucl. Phys. B240 (1984) 189, 533; B244 (1984)  
262; Phys. Lett. B142 (1984) 410.
- [12] A. Hanany, M. Strassler and A. Zaffaroni, Nucl. Phys. B513 (1998) 87 (hep-th/9707244).  
M. Strassler, Nucl. Phys. Proc. Suppl. 73 (1999) 120 (hep-lat/9810059).  
M. Strassler, Prog. Theor. Phys. Suppl. 131 (1998) 439 (hep-lat/9803009).
- [13] H. Meyer, JHEP 0401 (2004) 030 (hep-lat/0312034);  
JHEP 0301 (2003) 048 (hep-lat/0209145).
- [14] M. Luscher and P. Weisz, JHEP 0109 (2001) 010 (hep-lat/0108014).
- [15] B. Lucini, M. Teper and U. Wenger, hep-lat/0401028.
- [16] L. Del Debbio, H. Panagopoulos and E. Vicari, JHEP 0208 (2002) 044 (hep-th/0204125).
- [17] N. Cundy, M. Teper and U. Wenger, Phys. Rev. D66 (2002) 094505 (hep-lat/0203030).
- [18] H. Meyer and M. Teper, Nucl. Phys. B668 (2003) 111 (hep-lat/0306019), hep-lat/0308035  
and in progress.
- [19] J. Hoek, M. Teper and J. Waterhouse, Nucl. Phys. B288 (1987) 589.
- [20] S. Deldar, Phys. Rev. D62 (2000) 034509 (hep-lat/9911008).
- [21] G. Bali, Phys. Rev. D62 (2000) 114503 (hep-lat/0006022).
- [22] M. Teper, in *Large N QCD* (Ed. R.F. Lebed, World Scientific 2002)  
(hep-ph/0203203).
- [23] A. Armoni and M. Shifman, Nucl. Phys. B671 (2003) 67 (hep-th/0307020).

|              |       | $am_{eff}(n_t)$ |           |                |            |
|--------------|-------|-----------------|-----------|----------------|------------|
| state        | $n_t$ | $Q \simeq 0$    | $ Q  = 1$ | $ Q  \simeq 2$ | <i>all</i> |
| $G_{0^{++}}$ | 1     | 0.81(3)         | 0.81(1)   | 0.82(3)        | 0.80(1)    |
|              | 2     | 0.71(5)         | 0.78(3)   | 0.79(6)        | 0.76(2)    |
| $l_{k=1}$    | 1     | 0.75(1)         | 0.75(1)   | 0.76(1)        | 0.75(1)    |
|              | 2     | 0.71(2)         | 0.71(1)   | 0.76(2)        | 0.72(1)    |
| $l_{k=2}$    | 1     | 1.43(2)         | 1.41(1)   | 1.41(2)        | 1.42(1)    |
|              | 2     | 1.39(7)         | 1.32(3)   | 1.38(12)       | 1.34(3)    |

Table 1: Effective masses at  $t = n_t a$  for the lightest  $0^{++}$  glueball and the lightest  $k = 1$  and  $k = 2$  winding strings, on a  $12^4$  lattice at  $\beta = 44.85$  in  $SU(8)$ . The masses have been calculated separately for sequences of fields with the indicated topological charges.

| blocking + smearing : $SU(3)$ at $\beta = 5.9$ |     |        |     |     |        |     |     |        |     |     |        |
|--|-----|--------|-----|-----|--------|-----|-----|--------|-----|-----|--------|
| $b$  | $s$ | $m(a)$ | $b$ | $s$ | $m(a)$ | $b$ | $s$ | $m(a)$ | $b$ | $s$ | $m(a)$ |
| 0  | 0   | 2.28   | 1   | 0   | 1.40   | 2   | 0   | 0.99   | 3   | 0   | 1.05   |
| 0  | 2   | 1.72   | 1   | 2   | 1.15   | 2   | 2   | 0.92   | 3   | 2   | 1.09   |
| 0  | 4   | 1.49   | 1   | 4   | 1.04   | 2   | 4   | 0.91   | 3   | 4   | 1.12   |
| 0  | 6   | 1.35   | 1   | 6   | 0.97   | 2   | 6   | 0.93   | 3   | 6   | 1.14   |
| 0  | 8   | 1.25   | 1   | 8   | 0.94   | 2   | 8   | 0.96   | 3   | 8   | 1.15   |
| 0  | 10  | 1.19   | 1   | 10  | 0.93   | 2   | 10  | 1.00   | 3   | 10  | 1.16   |
| 0  | 12  | 1.14   | 1   | 12  | 0.93   | 2   | 12  | 1.04   | 3   | 12  | 1.17   |
| 0  | 14  | 1.10   | 1   | 14  | 0.93   | 2   | 14  | 1.09   | 3   | 14  | 1.17   |
| 0  | 0   | 2.26   | 1   | 0   | 1.38   | 2   | 0   | 0.95   | 3   | 0   | 1.07   |

Table 2: Effective  $0^{++}$  glueball masses at  $t = a$  for operators that are  $1 \times 1$  loops of (super)links blocked  $b$  times and then smeared  $s$  times. Parameters  $p_a = 1.0$  for blocking and  $p_a = 0.10$  for smearing. Last row is from a separate calculation with improved blocking with  $p_a = 0.40$  and  $p_d = 0.16$ . The calculation is for  $SU(3)$  on a  $12^4$  lattice at  $\beta = 5.9$ .

| Improved blocking : SU(4) at $\beta = 10.9$ |       |  |                |                |           |           |
|---|-------|--|----------------|----------------|-----------|-----------|
| parameters                                  |       | lightest effective masses at $t = a$ : |                |                |           |           |
| $p_a$                                       | $p_d$ | $l_{k=1}(p=0)$                         | $l_{k=1}(p=1)$ | $l_{k=2}(p=0)$ | $G_{0++}$ | $G_{2++}$ |
| 0.15  | 0.03  | 0.707(16)                              | 1.147(7)       | 1.068(34)      | 0.915(17) | 1.395(25) |
| 0.20  | 0.04  | 0.659(15)                              | 1.076(6)       | 0.973(30)      | 0.820(17) | 1.249(23) |
| 0.25  | 0.05  | 0.639(15)                              | 1.048(6)       | 0.936(32)      | 0.780(19) | 1.188(22) |
| 0.30  | 0.06  | 0.630(15)                              | 1.036(6)       | 0.919(31)      | 0.762(19) | 1.163(22) |
| 0.35  | 0.07  | 0.626(15)                              | 1.031(6)       | 0.909(31)      | 0.754(19) | 1.153(22) |
| 0.40  | 0.08  | 0.623(15)                              | 1.029(6)       | 0.903(31)      | 0.749(19) | 1.149(22) |
| 0.50  | 0.10  | 0.620(15)                              | 1.027(6)       | 0.897(31)      | 0.744(19) | 1.149(22) |
| 0.60  | 0.12  | 0.619(15)                              | 1.027(6)       | 0.894(31)      | 0.742(19) | 1.150(22) |
| 0.75  | 0.15  | 0.619(15)                              | 1.029(6)       | 0.892(31)      | 0.741(19) | 1.154(22) |
| 0.15  | 0.06  | 0.632(9)                               | 1.029(7)       | 0.937(20)      | 0.830(23) | 1.258(37) |
| 0.20  | 0.08  | 0.616(9)                               | 1.010(7)       | 0.904(20)      | 0.796(23) | 1.196(40) |
| 0.25  | 0.10  | 0.611(10)                              | 1.006(8)       | 0.893(20)      | 0.786(23) | 1.180(39) |
| 0.30  | 0.12  | 0.609(10)                              | 1.006(8)       | 0.888(19)      | 0.782(23) | 1.176(37) |
| 0.35  | 0.14  | 0.608(10)                              | 1.007(8)       | 0.886(19)      | 0.781(23) | 1.175(34) |
| 0.40  | 0.16  | 0.608(10)                              | 1.008(8)       | 0.885(19)      | 0.780(23) | 1.175(32) |
| 0.50  | 0.20  | 0.608(10)                              | 1.011(8)       | 0.884(19)      | 0.779(23) | 1.176(30) |
| 0.60  | 0.24  | 0.608(10)                              | 1.013(8)       | 0.883(19)      | 0.779(23) | 1.177(29) |
| 0.75  | 0.30  | 0.608(10)                              | 1.015(8)       | 0.883(19)      | 0.780(23) | 1.178(28) |
| 0.25  | 0.15  | 0.608(10)                              | 1.009(8)       | 0.884(19)      | 0.781(23) | 1.175(34) |
| 0.35  | 0.21  | 0.608(10)                              | 1.012(8)       | 0.882(19)      | 0.780(22) | 1.175(30) |
| 0.50  | 0.30  | 0.609(10)                              | 1.016(8)       | 0.883(19)      | 0.780(22) | 1.177(28) |
| 0.75  | 0.45  | 0.610(10)                              | 1.022(8)       | 0.884(19)      | 0.781(22) | 1.179(28) |

Table 3: How improved blocking varies with parameters. Effective masses at  $t = a$  of periodic  $k = 1$  and  $k = 2$  strings, and the  $t = a$  energy of the  $k = 1$  string with lowest non-zero momentum. Also the lightest scalar and tensor glueballs. Calculations are in SU(4) on a  $12^4$  lattice at  $\beta = 10.9$ . From the best operators formed out of (super)links using improved blocking and the various blocking parameters shown.

| Best Overlaps in SU(4) |           |           |              |                   |           |           |              |
|------------------------|-----------|-----------|--------------|-------------------|-----------|-----------|--------------|
| Old blocking [1]       |           |           |              | Improved blocking |           |           |              |
| $\beta$                | $l_{k=1}$ | $l_{k=2}$ | $G_{0^{++}}$ | $\beta$           | $l_{k=1}$ | $l_{k=2}$ | $G_{0^{++}}$ |
| 10.55                  | 0.69      | 0.59      | 0.90         | 10.55             | 0.968     | 0.945     | 0.963        |
| 10.70                  | 0.81      | 0.67      | 0.89         | 10.70             | 0.967     | 0.937     | 0.973        |
| 10.90                  | 0.84      | 0.71      | 0.76         | 10.87             | 0.975     | 0.951     | 0.963        |
| 11.10                  | 0.77      | 0.59      | 0.84         | 11.085            | 0.965     | 0.941     | 0.963        |
| 11.30                  | 0.79      | 0.62      | 0.86         | 11.40             | 0.981     | 0.962     | 0.965        |

Table 4: Best overlaps for the lightest  $k = 1$  and  $k = 2$  loops and the  $0^{++}$  glueball. From the old blocking calculation of [1] and from the improved blocking calculation of this paper.

| SU(2)   |     |                  |               |                |               |
|---------|-----|------------------|---------------|----------------|---------------|
| $\beta$ | $L$ | $a\sqrt{\sigma}$ | $am_{0^{++}}$ | $am_{0^{++*}}$ | $am_{2^{++}}$ |
| 2.1768  | 8   | 0.5149(77)       | 1.626(57)     | 2.65(48)       | 2.73(45)      |
| 2.2986  | 10  | 0.3667(18)       | 1.212(22)     | 2.00(11)       | 1.95(9)       |
| 2.3715  | 12  | 0.2879(13)       | 0.994(18)     | 1.64(7)        | 1.56(5)       |
| 2.3726  | 12  | 0.2879(10)       | 1.015(13)     | 1.60(5)        | 1.562(29)     |
| 2.4265  | 16  | 0.2388(9)        | 0.834(13)     | 1.47(4)        | 1.340(27)     |
| 2.5115  | 20  | 0.1768(8)        | 0.658(10)     | 1.100(17)      | 0.954(13)     |

Table 5: The string tension, the lightest and first excited  $J^{PC} = 0^{++}$  glueball masses and the lightest  $2^{++}$  glueball mass: calculated at the indicated values of  $\beta$  on  $L^4$  lattices in SU(2).

| SU(3)   |     |                  |               |                |               |
|---------|-----|------------------|---------------|----------------|---------------|
| $\beta$ | $L$ | $a\sqrt{\sigma}$ | $am_{0^{++}}$ | $am_{0^{++*}}$ | $am_{2^{++}}$ |
| 5.6925  | 8   | 0.3970(19)       | 0.941(25)     | 1.99(12)       | 2.01(14)      |
| 5.6993  | 8   | 0.3933(16)       | 0.969(18)     | 2.12(14)       | 1.97(12)      |
| 5.7995  | 10  | 0.3148(12)       | 0.909(15)     | 1.65(6)        | 1.52(5)       |
| 5.8000  | 10  | 0.3133(13)       | 0.945(21)     | 1.58(8)        | 1.57(6)       |
| 5.8945  | 12  | 0.2607(11)       | 0.795(13)     | 1.42(4)        | 1.279(22)     |
| 6.0625  | 16  | 0.19466(73)      | 0.648(11)     | 1.073(16)      | 0.922(13)     |
| 6.3380  | 24  | 0.12930(69)      | 0.448(11)     | 0.731(13)      | 0.636(12)     |

Table 6: The string tension, the lightest and first excited  $J^{PC} = 0^{++}$  glueball masses and the lightest  $2^{++}$  glueball mass: calculated at the indicated values of  $\beta$  on  $L^4$  lattices in SU(3).

| SU(4)   |     |                  |               |                |               |
|---------|-----|------------------|---------------|----------------|---------------|
| $\beta$ | $L$ | $a\sqrt{\sigma}$ | $am_{0^{++}}$ | $am_{0^{++*}}$ | $am_{2^{++}}$ |
| 10.550  | 8   | 0.3739(15)       | 0.819(21)     | 1.626(73)      | 1.66(7)       |
| 10.637  | 10  | 0.3254(6)        | 0.864(9)      | 1.652(44)      | 1.575(40)     |
| 10.700  | 10  | 0.2977(13)       | 0.839(17)     | 1.425(56)      | 1.427(50)     |
| 10.789  | 12  | 0.2706(8)        | 0.788(12)     | 1.440(35)      | 1.305(35)     |
| 10.870  | 12  | 0.2467(11)       | 0.746(16)     | 1.357(33)      | 1.185(28)     |
| 11.085  | 16  | 0.19868(83)      | 0.618(13)     | 1.093(19)      | 0.981(19)     |
| 11.400  | 20  | 0.15277(72)      | 0.476(11)     | 0.825(15)      | 0.736(15)     |

Table 7: The string tension, the lightest and first excited  $J^{PC} = 0^{++}$  glueball masses and the lightest  $2^{++}$  glueball mass: calculated at the indicated values of  $\beta$  on  $L^4$  lattices in SU(4).

| SU(6)   |     |                  |               |                |               |
|---------|-----|------------------|---------------|----------------|---------------|
| $\beta$ | $L$ | $a\sqrt{\sigma}$ | $am_{0^{++}}$ | $am_{0^{++*}}$ | $am_{2^{++}}$ |
| 24.350  | 8   | 0.3886(18)       | 0.764(24)     | 1.77(11)       | 1.83(11)      |
| 24.500  | 10  | 0.3416(18)       | 0.837(21)     | 1.731(73)      | 1.60(6)       |
| 24.515  | 10  | 0.3385(15)       | 0.856(20)     | 1.643(75)      | 1.57(6)       |
| 24.670  | 10  | 0.3075(14)       | 0.812(19)     | 1.509(65)      | 1.438(47)     |
| 24.845  | 12  | 0.2801(13)       | 0.774(13)     | 1.514(50)      | 1.315(35)     |
| 25.050  | 12  | 0.2510(10)       | 0.727(16)     | 1.316(54)      | 1.181(35)     |
| 25.452  | 16  | 0.20992(82)      | 0.613(12)     | 1.150(24)      | 0.989(20)     |

Table 8: The string tension, the lightest and first excited  $J^{PC} = 0^{++}$  glueball masses and the lightest  $2^{++}$  glueball mass: calculated at the indicated values of  $\beta$  on  $L^4$  lattices in SU(6).

| SU(8)   |     |                  |               |                |               |
|---------|-----|------------------|---------------|----------------|---------------|
| $\beta$ | $L$ | $a\sqrt{\sigma}$ | $am_{0^{++}}$ | $am_{0^{++*}}$ | $am_{2^{++}}$ |
| 43.85   | 8   | 0.3630(21)       | 0.835(30)     | 1.63(16)       | 1.64(12)      |
| 44.00   | 10  | 0.3413(13)       | 0.829(20)     | 1.59(7)        | 1.64(6)       |
| 44.35   | 10  | 0.3008(14)       | 0.804(23)     | 1.36(7)        | 1.39(6)       |
| 44.85   | 12  | 0.2598(12)       | 0.776(19)     | 1.46(5)        | 1.22(3)       |
| 45.70   | 16  | 0.2090(13)       | 0.632(23)     | 1.18(4)        | 0.99(3)       |

Table 9: The string tension, the lightest and first excited  $J^{PC} = 0^{++}$  glueball masses and the lightest  $2^{++}$  glueball mass: calculated at the indicated values of  $\beta$  on  $L^4$  lattices in SU(8).

| SU(4)   |                   |                   | SU(6)   |                   |                   |                   |
|---------|-------------------|-------------------|---------|-------------------|-------------------|-------------------|
| $\beta$ | $a^2\sigma_{k=1}$ | $a^2\sigma_{k=2}$ | $\beta$ | $a^2\sigma_{k=1}$ | $a^2\sigma_{k=2}$ | $a^2\sigma_{k=3}$ |
| 10.550  | 0.1398(11)        | 0.1900(30)        | 24.350  | 0.1510(14)        | 0.2511(70)        | 0.264(12)         |
| 10.637  | 0.10588(38)       | 0.1459(14)        | 24.500  | 0.1167(12)        | 0.1885(40)        | 0.2222(87)        |
| 10.700  | 0.08863(77)       | 0.1186(17)        | 24.515  | 0.1146(11)        | 0.1913(40)        | 0.2145(84)        |
| 10.789  | 0.07321(40)       | 0.10160(83)       | 24.670  | 0.09453(76)       | 0.1551(23)        | 0.1787(47)        |
| 10.870  | 0.06087(51)       | 0.08286(108)      | 24.845  | 0.07846(65)       | 0.1300(13)        | 0.1469(34)        |
| 11.085  | 0.03947(34)       | 0.05433(80)       | 25.050  | 0.06299(50)       | 0.1030(13)        | 0.1201(24)        |
| 11.400  | 0.02334(22)       | 0.03157(49)       | 25.452  | 0.04407(34)       | 0.07398(77)       | 0.0829(14)        |

Table 10: Tensions of  $k$ -strings in our SU(4) and SU(6) calculations.

| SU(8)   |                   |                   |                   |                   |
|---------|-------------------|-------------------|-------------------|-------------------|
| $\beta$ | $a^2\sigma_{k=1}$ | $a^2\sigma_{k=2}$ | $a^2\sigma_{k=3}$ | $a^2\sigma_{k=4}$ |
| 43.85   | 0.1318(15)        | 0.2317(56)        | 0.276(18)         | 0.296(32)         |
| 44.00   | 0.11646(91)       | 0.2107(54)        | 0.256(14)         | 0.271(31)         |
| 44.35   | 0.09049(83)       | 0.1580(26)        | 0.2012(68)        | 0.215(12)         |
| 44.85   | 0.06750(64)       | 0.1184(25)        | 0.1541(40)        | 0.1548(60)        |
| 45.70   | 0.04370(50)       | 0.0782(12)        | 0.1003(19)        | 0.1135(38)        |

Table 11: Tensions of  $k$ -strings in our SU(8) calculations.

| SU(4) anisotropic: $\xi = 0.5$ |           |               |               |                  |                   |                  |
|--------------------------------|-----------|---------------|---------------|------------------|-------------------|------------------|
| $\beta$                        | lattice   | $a_t m_{k=1}$ | $a_t m_{k=2}$ | $a_t m_{0^{++}}$ | $a_t m_{0^{++*}}$ | $a_t m_{2^{++}}$ |
| 10.700                         | $8^3 20$  | 0.4021(36)    | 0.5692(68)    | 0.3920(73)       | 0.827(14)         | 0.750(25)        |
| 10.850                         | $10^3 26$ | 0.3516(43)    | 0.5100(81)    | 0.3697(55)       | 0.724(13)         | 0.630(15)        |
| 11.050                         | $12^3 30$ | 0.2878(26)    | 0.4048(64)    | 0.3234(84)       | 0.616(17)         | 0.507(13)        |
| 11.325                         | $16^3 40$ | 0.2400(21)    | 0.3347(69)    | 0.2767(82)       | 0.558(18)         | 0.417(8)         |

Table 12: Masses of the lightest  $k = 1$  and  $k = 2$  winding strings, of the lightest and first excited  $J^{PC} = 0^{++}$  glueball masses and of the lightest  $2^{++}$  glueball. Calculated in SU(4) with a bare anisotropy  $\xi = a_t/a_s = 0.5$  at the indicated values of  $\beta$  on the lattices shown.

| SU(4) anisotropic : $\xi = 0.5$ |          |                    |                             |                         |                          |                         |
|---------------------------------|----------|--------------------|-----------------------------|-------------------------|--------------------------|-------------------------|
| $\beta$                         | $\xi_r$  | $a_t\sqrt{\sigma}$ | $\sigma_{k=2}/\sigma_{k=1}$ | $m_{0++}/\sqrt{\sigma}$ | $m_{0+++}/\sqrt{\sigma}$ | $m_{2++}/\sqrt{\sigma}$ |
| 10.700                          | 0.405(5) | 0.1518(12)         | 1.367(19)                   | 2.582(52)               | 5.45(10)                 | 4.94(17)                |
| 10.850                          | 0.408(8) | 0.1268(15)         | 1.402(26)                   | 2.916(56)               | 5.71(13)                 | 4.97(13)                |
| 11.050                          | 0.415(4) | 0.10586(67)        | 1.361(24)                   | 3.055(82)               | 5.82(17)                 | 4.79(13)                |
| 11.325                          | 0.430(6) | 0.08489(68)        | 1.353(28)                   | 3.260(99)               | 6.57(22)                 | 4.91(10)                |
| $\infty$                        |          |                    | 1.358(33)                   | 3.56(11)                | 6.60(23)*                | 4.85(16)                |

Table 13: The renormalised anisotropy,  $\xi_r$ , the string tension and mass ratios from the masses in Table 12. With the results of the continuum extrapolations. (The  $\star$  indicates a poor fit.)

| continuum limit     |                         |                          |                         |
|---------------------|-------------------------|--------------------------|-------------------------|
|                     | $m_{0++}/\sqrt{\sigma}$ | $m_{0+++}/\sqrt{\sigma}$ | $m_{2++}/\sqrt{\sigma}$ |
| SU(2)               | 3.78(7)                 | 6.46(14)                 | 5.45(11)                |
| SU(3)               | 3.55(7)                 | 5.69(10)                 | 4.78(9)                 |
| SU(4)               | 3.36(6)                 | 5.63(12)*                | 4.88(11)                |
| SU(4) <sub>an</sub> | 3.56(11)                | 6.60(23)*                | 4.85(16)                |
| SU(6)               | 3.25(9)                 | 5.84(18)                 | 4.73(15)                |
| SU(8)               | 3.55(12)                | 6.40(30)*                | 4.73(22)                |
| SU( $\infty$ )      | 3.307(53)               | 6.07(17)                 | 4.80(14)                |

Table 14: The continuum limit of the lightest scalar and tensor glueball masses, and the first excited scalar mass, all in units of the string tension  $\sigma$ . (The  $\star$  label denotes a poor fit.) The extrapolation of these to  $N = \infty$  is shown.

| $L = 16 ; a \simeq 0.2/\sqrt{\sigma}$ |                         |                          |                         |
|---------------------------------------|-------------------------|--------------------------|-------------------------|
|                                       | $m_{0++}/\sqrt{\sigma}$ | $m_{0+++}/\sqrt{\sigma}$ | $m_{2++}/\sqrt{\sigma}$ |
| SU(2)                                 | 3.493(56)               | 6.16(17)                 | 5.61(12)                |
| SU(3)                                 | 3.329(58)               | 5.51(9)                  | 4.74(7)                 |
| SU(4)                                 | 3.111(67)               | 5.49(11)                 | 4.94(10)                |
| SU(6)                                 | 2.920(59)               | 5.48(12)                 | 4.71(10)                |
| SU(8)                                 | 3.024(112)              | 5.65(20)                 | 4.74(15)                |
| SU( $\infty$ )                        | 2.84(7)                 | 5.52(13)                 | 4.78(11)                |

Table 15: The masses of the lightest scalar and tensor glueballs, and the first excited scalar, in units of the string tension  $\sigma$ , as calculated at the smallest value of  $a$  that is ‘common’ to all  $N$ . The value of  $a\sqrt{\sigma}$  lies in the range [0.195,0.210] except for SU(2) where it is  $\sim 0.24$ . The extrapolation of these to  $N = \infty$  is shown.

| $\sigma_k/\sigma$ |                 |            |        |
|-------------------|-----------------|------------|--------|
| (N,k)             | Casimir scaling | this paper | 'MQCD' |
| (4,2)             | 1.333           | 1.370(20)  | 1.414  |
| (4,2)             | 1.333           | 1.358(33)  | 1.414  |
| (6,2)             | 1.600           | 1.675(31)  | 1.732  |
| (6,3)             | 1.800           | 1.886(61)  | 2.000  |
| (8,2)             | 1.714           | 1.779(51)  | 1.848  |
| (8,3)             | 2.143           | 2.38(10)   | 2.414  |
| (8,4)             | 2.286           | 2.69(17)   | 2.613  |

Table 16: Predictions of ‘Casimir Scaling’ and ‘MQCD’ compared against our calculated values of the ratio of the tension of the lightest  $k$ -string to that of the fundamental ( $k = 1$ ) string. The second SU(4) calculation is the one on the anisotropic lattice.

| string masses |           |       |           |       |           |       |
|---------------|-----------|-------|-----------|-------|-----------|-------|
|               | SU(4)     |       | SU(6)     |       | SU(8)     |       |
| $k$           | $am$      | CS    | $am$      | CS    | $am$      | CS    |
| 1             | 0.566(6)  | 0.566 | 0.640(6)  | 0.640 | 0.634(8)  | 0.634 |
| 2A            | 0.804(10) | 0.777 | 1.118(13) | 1.063 | 1.186(18) | 1.133 |
| 2S            | 1.235(20) | 1.451 | 1.411(21) | 1.547 | 1.443(23) | 1.488 |
| 3A            |           |       | 1.281(16) | 1.204 | 1.542(29) | 1.433 |
| 3S            |           |       | 2.16(10)  | 2.656 | 2.19(13)  | 2.498 |
| 3M            |           |       | 1.863(50) | 1.930 | 1.97(6)   | 1.966 |

Table 17: Our mass estimates for strings in various representations, compared to the Casimir Scaling prediction obtained by scaling up the  $k = 1$  mass, assuming the leading string correction. All from the isotropic  $16^4$  lattice calculations at the smallest value of  $a$ .

| $am_k(n_t)$ |         |          |            |         |          |            |         |          |            |
|-------------|---------|----------|------------|---------|----------|------------|---------|----------|------------|
|             | SU(4)   |          |            | SU(6)   |          |            | SU(8)   |          |            |
| $n_t$       | $k = 1$ | $k = 2S$ | $k = 2A^*$ | $k = 1$ | $k = 2S$ | $k = 2A^*$ | $k = 1$ | $k = 2S$ | $k = 2A^*$ |
| 1           | 0.60(1) | 1.40(1)  | 1.40(1)    | 0.67(1) | 1.54(1)  | 1.67(1)    | 0.66(1) | 1.51(1)  | 1.69(1)    |
| 2           | 0.57(1) | 1.25(2)  | 1.30(2)    | 0.64(1) | 1.42(2)  | 1.55(2)    | 0.64(1) | 1.42(2)  | 1.53(3)    |
| 3           | 0.56(1) | 1.22(4)  | 1.25(7)    | 0.63(1) | 1.39(6)  | 1.57(8)    | 0.63(1) | 1.56(7)  | 1.54(12)   |

Table 18: Effective masses versus  $t = an_t$  for  $k = 1$  and  $k = 2$  strings in the representations shown. (Errors rounded up.) From isotropic  $16^4$  lattices at our smallest lattice spacing.

| SU(6) : $am_k(n_t)$ |          |          |            |            |               |
|---------------------|----------|----------|------------|------------|---------------|
| $n_t$               | $k = 3S$ | $k = 3M$ | $k = 3M^*$ | $k = 3A^*$ | $k = 3A^{**}$ |
| 1                   | 2.55(1)  | 2.03(2)  | 2.46(1)    | 1.94(1)    | 2.74(2)       |
| 2                   | 2.16(10) | 1.86(5)  | 2.21(9)    | 1.77(4)    | 2.38(19)      |

Table 19: Effective masses versus  $t = an_t$  for  $k = 3$  strings in the representations shown. (Errors rounded up.) From isotropic  $16^4$  lattices at our smallest lattice spacing.

| SU(8) : $am_k(n_t)$ |          |          |            |            |               |
|---------------------|----------|----------|------------|------------|---------------|
| $n_t$               | $k = 3S$ | $k = 3M$ | $k = 3M^*$ | $k = 3A^*$ | $k = 3A^{**}$ |
| 1                   | 2.50(2)  | 2.08(2)  | 2.52(2)    | 2.15(1)    | 3.17(3)       |
| 2                   | 2.19(13) | 1.97(6)  | 2.17(12)   | 1.93(7)    | 2.53(28)      |

Table 20: Effective masses versus  $t = an_t$  for  $k = 3$  strings in the representations shown. (Errors rounded up.) From isotropic  $16^4$  lattices at our smallest lattice spacing.

| SU(4) : $am_k(a)$ |             |          |          |          |           |         |          |          |
|-------------------|-------------|----------|----------|----------|-----------|---------|----------|----------|
| state             | anisotropic |          |          |          | isotropic |         |          |          |
|                   | $k = 1$     | $k = 2$  | $k = 2A$ | $k = 2S$ | $k = 1$   | $k = 2$ | $k = 2A$ | $k = 2S$ |
| 1                 | 0.320(1)    | 0.388(2) | 0.388(2) | 0.787(2) | 0.60(1)   | 0.86(1) | 0.86(1)  | 1.40(1)  |
| 2                 | 0.671(1)    | 0.779(2) | 0.779(2) | 1.258(3) | 1.27(1)   | 1.36(1) | 1.40(1)  | 1.87(1)  |
| 3                 | 1.063(2)    | 0.787(2) | 1.204(2) | 1.768(5) | 1.77(1)   | 1.49(1) | 1.98(1)  | 3.03(2)  |
| 4                 | 1.484(3)    | 1.204(2) | 1.649(5) | 2.299(6) | 3.31(2)   | 1.91(1) | 4.01(6)  | 6.6(5)   |
| 5                 | 1.929(5)    | 1.258(3) | 2.144(8) | 2.88(1)  |           | 2.00(1) |          |          |

Table 21: Effective masses at  $t = a$  for strings in SU(4) in the representations shown. The ground and excited states are listed in increasing order of mass. Shown separately are results from the anisotropic and isotropic lattices with the smallest lattice spacing.

| SU(6) : $am_k(a)$ |          |         |          |          |          |          |          |
|-------------------|----------|---------|----------|----------|----------|----------|----------|
| state             | $k = 1$  | $k = 2$ | $k = 2A$ | $k = 2S$ | $k = 3A$ | $k = 3M$ | $k = 3S$ |
| 1                 | 0.668(2) | 1.18(1) | 1.18(1)  | 1.54(1)  | 1.37(1)  | 2.03(2)  | 2.55(1)  |
| 2                 | 1.332(3) | 1.53(1) | 1.67(1)  | 1.99(1)  | 1.94(1)  | 2.46(1)  | 3.26(2)  |
| 3                 | 1.894(5) | 1.72(1) | 2.44(1)  | 3.26(2)  | 2.74(2)  | 3.95(4)  | 5.32(16) |
| 4                 | 3.61(3)  | 2.04(1) | 5.07(12) |          | 5.4(3)   | 6.5(6)   | 7.2(1.1) |

Table 22: Effective masses at  $t = a$  for strings in SU(6) in the representations shown. The ground and excited states are listed in increasing order of mass. From the  $16^4$  lattice at the smallest lattice spacing.

| SU(8) : $am_k(a)$ |          |         |          |          |          |          |          |
|-------------------|----------|---------|----------|----------|----------|----------|----------|
| state             | $k = 1$  | $k = 2$ | $k = 2A$ | $k = 2S$ | $k = 3A$ | $k = 3M$ | $k = 3S$ |
| 1                 | 0.658(3) | 1.24(1) | 1.25(1)  | 1.51(1)  | 1.64(1)  | 2.08(2)  | 2.50(2)  |
| 2                 | 1.320(4) | 1.51(1) | 1.69(1)  | 1.95(1)  | 2.15(1)  | 2.52(2)  | 3.11(3)  |
| 3                 | 1.887(8) | 1.74(1) | 2.54(2)  | 3.22(3)  | 3.17(3)  | 4.09(7)  | 5.20(21) |
| 4                 | 3.56(4)  | 2.01(1) | 5.5(4)   | 6.5(8)   | 6.3(8)   | 6.8(9)   | 6.1(6)   |

Table 23: Effective masses at  $t = a$  for strings in SU(8) in the representations shown. The ground and excited states are listed in increasing order of mass. From the  $16^4$  lattice at the smallest lattice spacing.

| $am_k(a)$ |                      |         |          |          |                      |           |           |           |
|-----------|----------------------|---------|----------|----------|----------------------|-----------|-----------|-----------|
| state     | SU(2) : $a = 1/8T_c$ |         |          |          | SU(3) : $a = 1/6T_c$ |           |           |           |
|           | $k = 1$              | $k = 2$ | $k = 2A$ | $k = 2S$ | $k = 1$              | $k = 2$   | $k = 2A$  | $k = 2S$  |
| 1         | 0.573(6)             | –       | –        | 1.20(6)  | 0.727(7)             | 0.726(8)  | 0.726(8)  | 1.641(33) |
| 2         | 1.100(12)            | –       | –        | 1.77(4)  | 1.56(4)              | 1.524(33) | 1.527(33) | 2.64(30)  |
| 3         | 1.40(10)             | –       | –        | 2.9(4)   | 2.25(20)             | 1.651(31) | 2.2(2)    | –         |
| 4         | 2.2(2)               | –       | –        | –        | –                    | 2.8(4)    | –         | –         |

Table 24: Effective masses for strings in SU(2) and in SU(3) in the representations shown. The ground and excited states are listed in increasing order of mass.

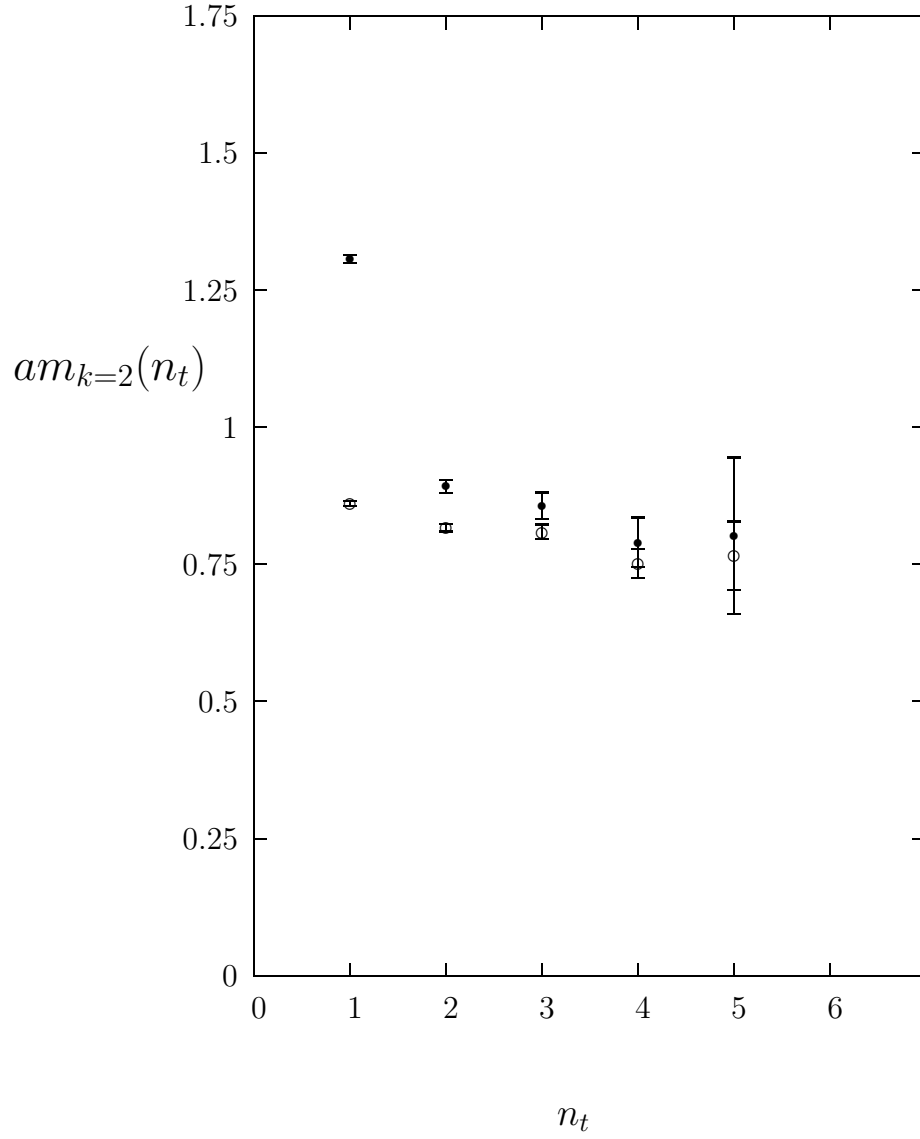


Figure 1: Effective mass of the SU(4)  $k = 2$  string as a function of  $n_t$  for a  $16^4$  lattice with old blocking,  $\bullet$ , and improved blocking,  $\circ$ . (The value of  $a$  differs by about 3% in the two calculations.)

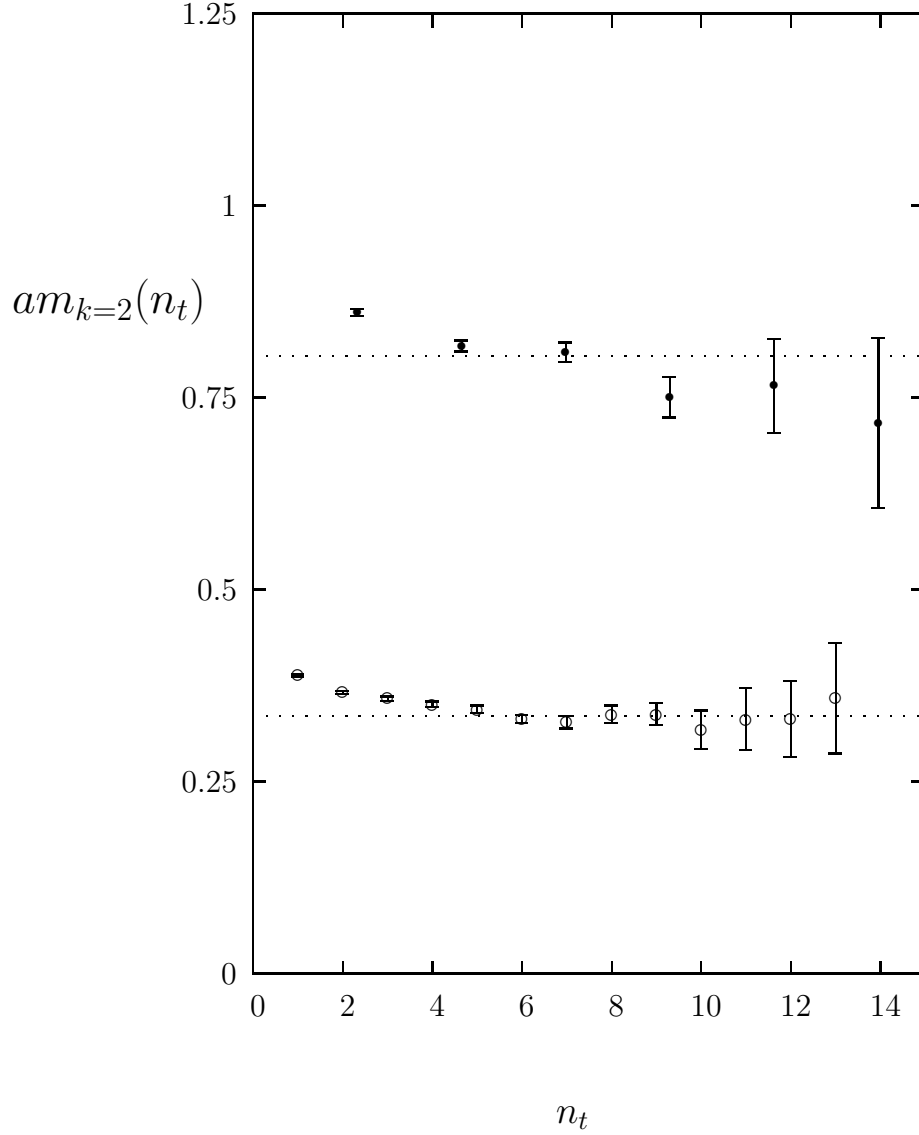


Figure 2: Effective mass of the SU(4)  $k = 2$  string as a function of  $n_t$  for an anisotropic lattice,  $\circ$ , and an isotropic lattice,  $\bullet$ , both with the same value of  $a_s$ ,  $a_s\sqrt{\sigma} \simeq 0.198$ , and  $L_s = 16$ . The value of  $n_t$  is for the anisotropic lattice, and the isotropic values of  $n_t$  have been scaled up by the calculated value of  $a_s/a_t$ .

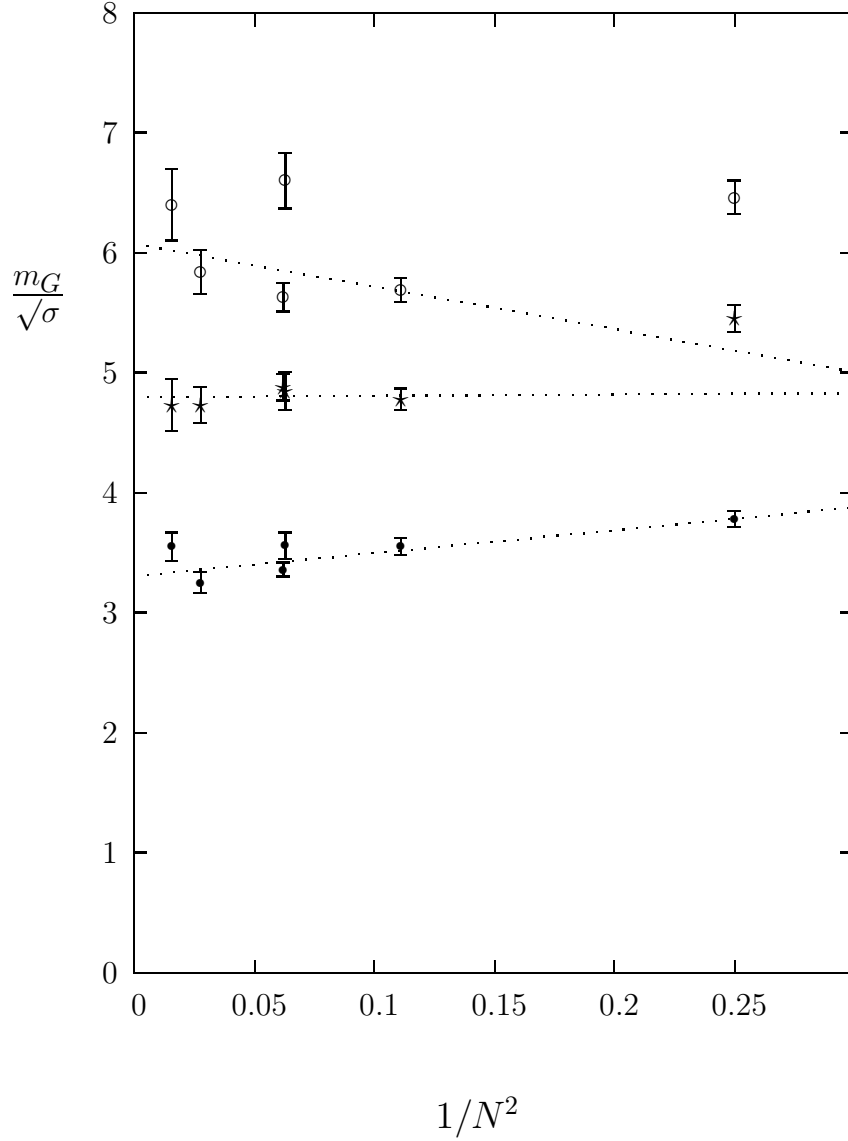


Figure 3: The lightest glueball masses expressed in units of the fundamental string tension, in the continuum limit, plotted against  $1/N^2$ . The  $0^{++}$ ,  $\bullet$ , the  $2^{++}$ ,  $\star$ , and the first excited  $0^{++*}$ ,  $\circ$ . Dotted lines are extrapolations to  $N = \infty$ .

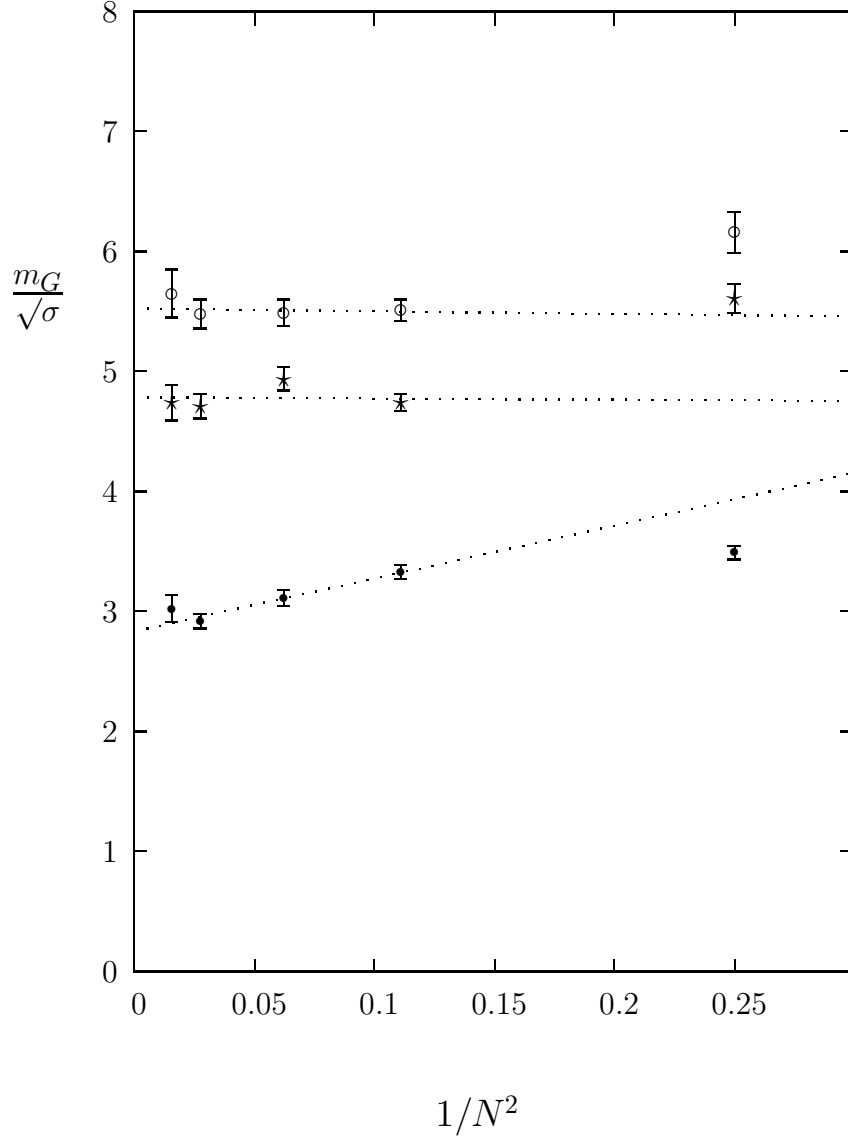


Figure 4: The lightest glueball masses expressed in units of the fundamental string tension plotted against  $1/N^2$ . The  $0^{++}$ , ●, the  $2^{++}$ , ★, and the first excited  $0^{++}$ , ○. Dotted lines are extrapolations to  $N = \infty$ . On  $16^4$  lattices with a nearly common value of the lattice spacing,  $a\sqrt{\sigma} \in [0.195, 0.210]$ , except for  $SU(2)$  where  $a\sqrt{\sigma} \simeq 0.24$ .

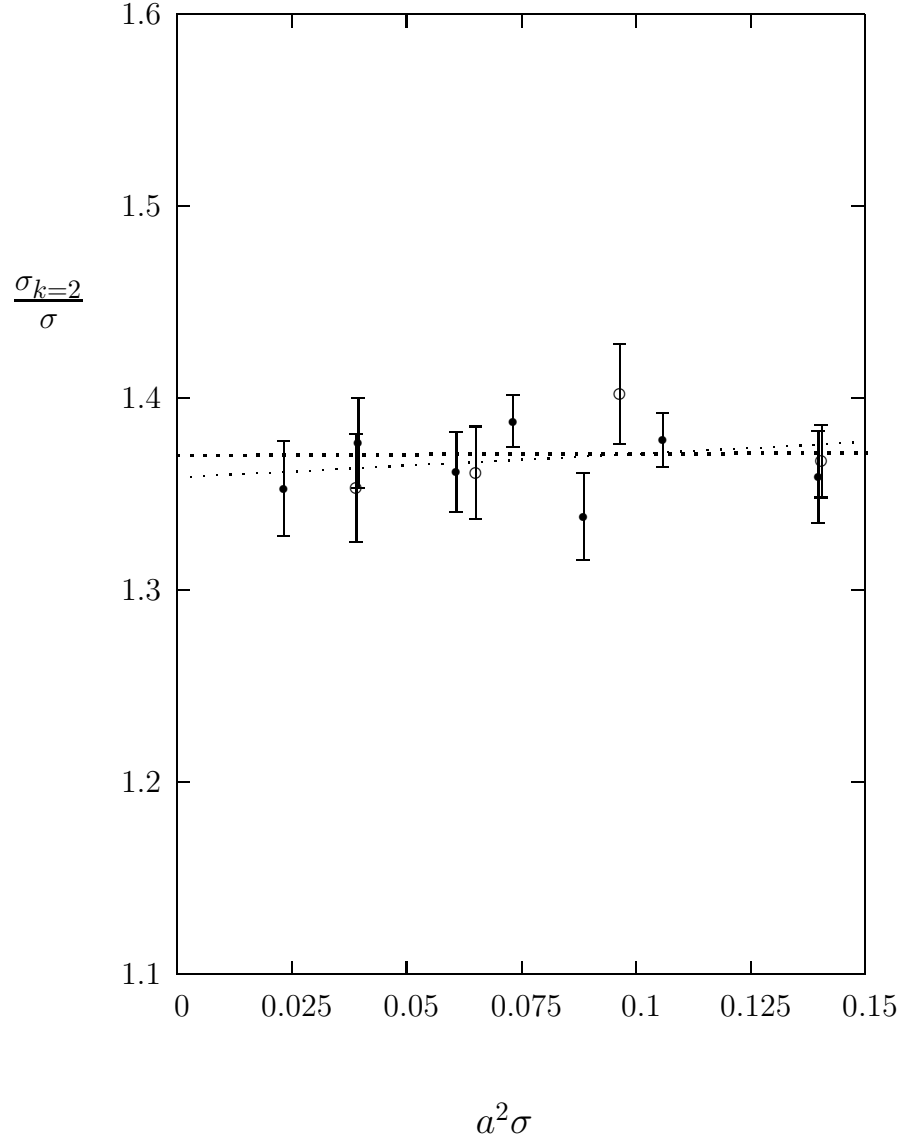


Figure 5: Ratio of the tension of the  $k = 2$  string to that of the fundamental ( $k = 1$ ) string in  $SU(4)$ , for the anisotropic ( $\circ$ ) and isotropic ( $\bullet$ ) calculations. Plotted against the square of the (spatial) lattice spacing. Continuum extrapolations are shown.

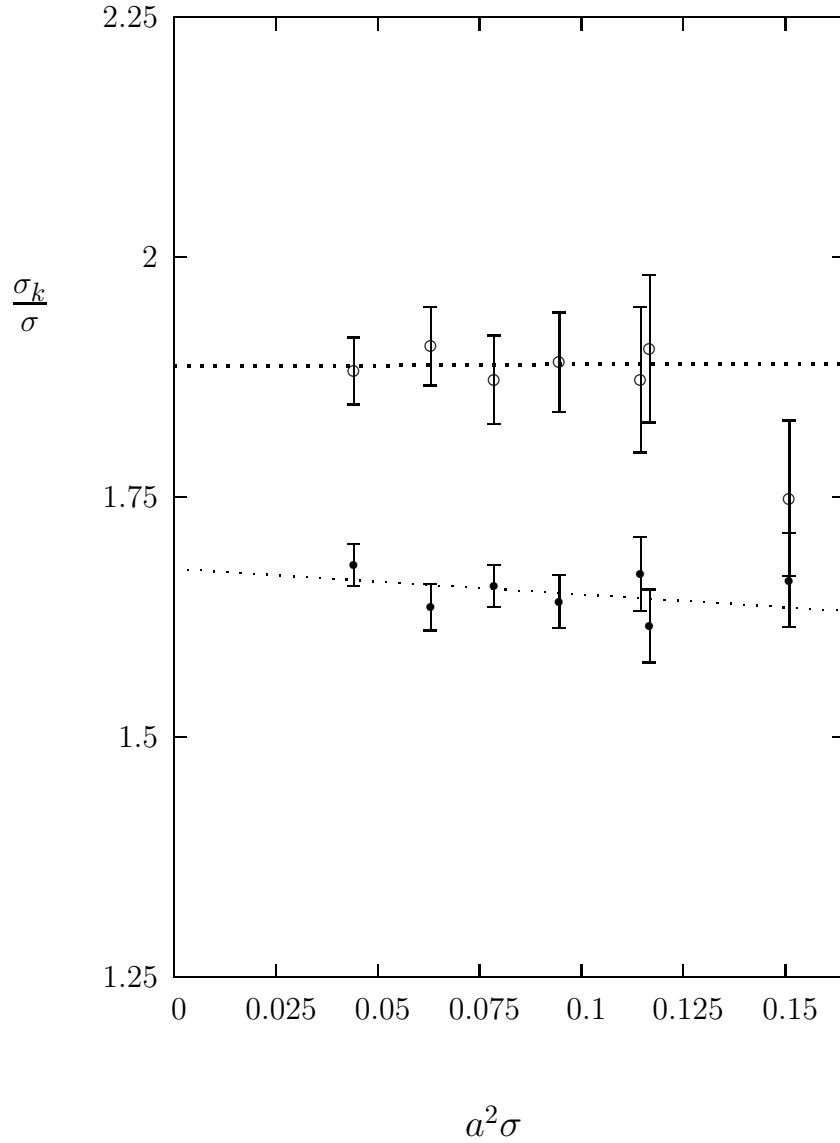


Figure 6: Ratio of the tensions of the  $k = 2$  ( $\bullet$ ) and  $k = 3$  ( $\circ$ ) strings to that of the fundamental ( $k = 1$ ) string in SU(6). Plotted against the square of the lattice spacing. Continuum extrapolations are shown.

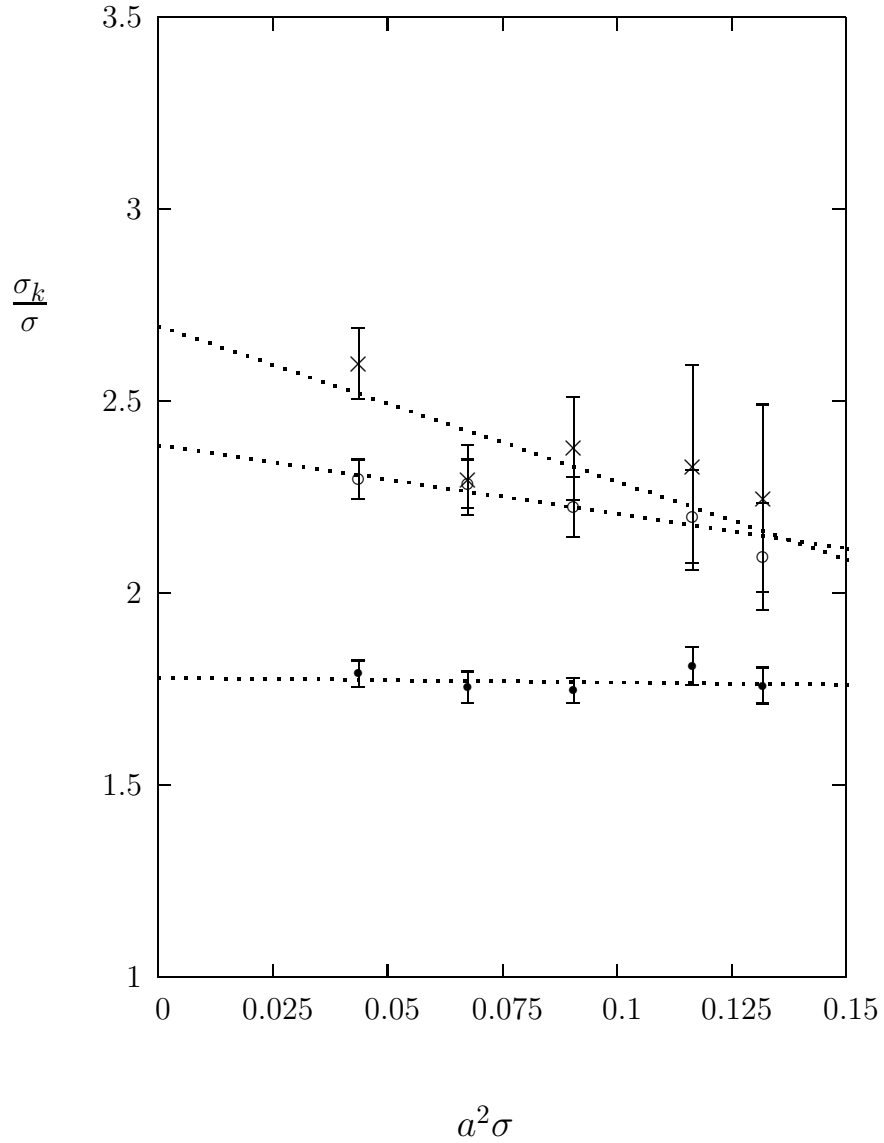


Figure 7: Ratio of the tensions of the  $k = 2$  (●),  $k = 3$  (○) and  $k = 4$  (×) strings to that of the fundamental ( $k = 1$ ) string in SU(8). Plotted against the square of the lattice spacing. Continuum extrapolations are shown.

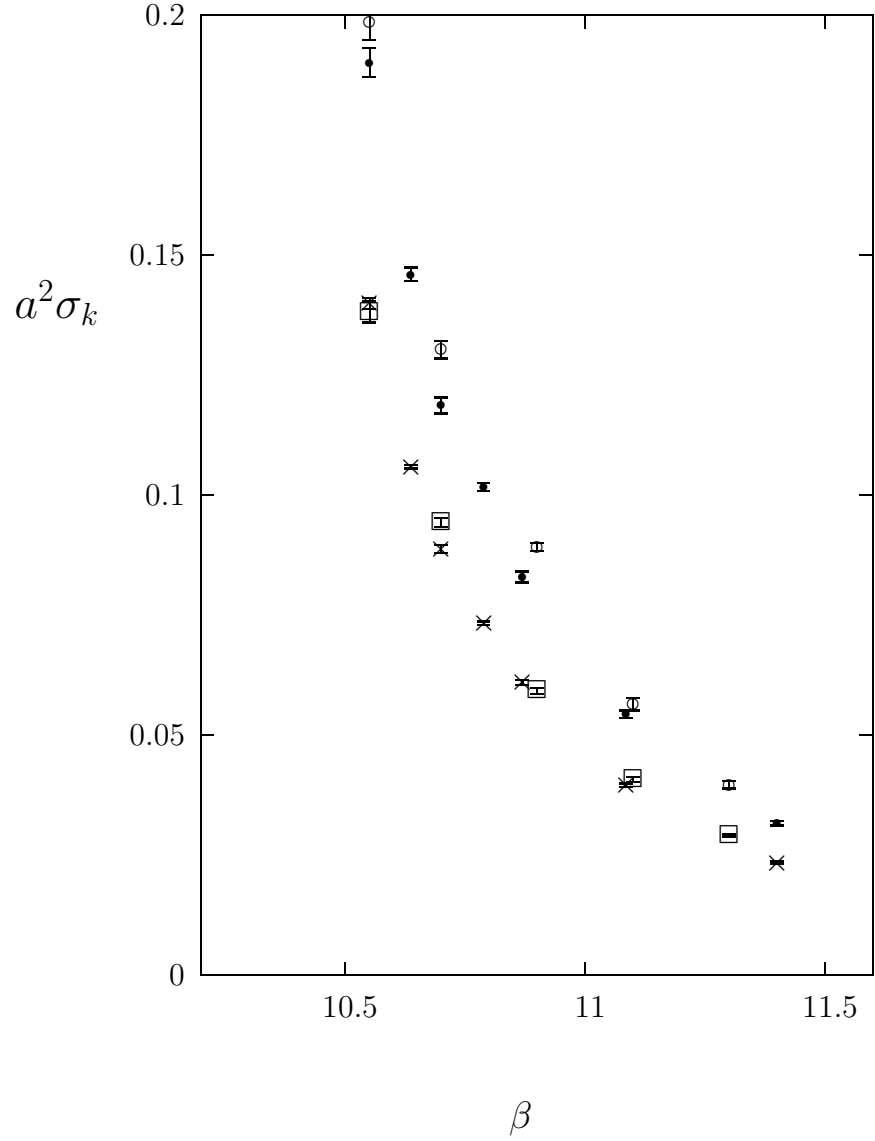


Figure 8: Comparison of the SU(4)  $k = 1$ ,  $k = 2$  string tensions obtained in this work ( $\times$ ,  $\bullet$  respectively) with those obtained in [1] ( $\square$ ,  $\circ$  respectively). Plotted against the inverse coupling  $\beta$ .

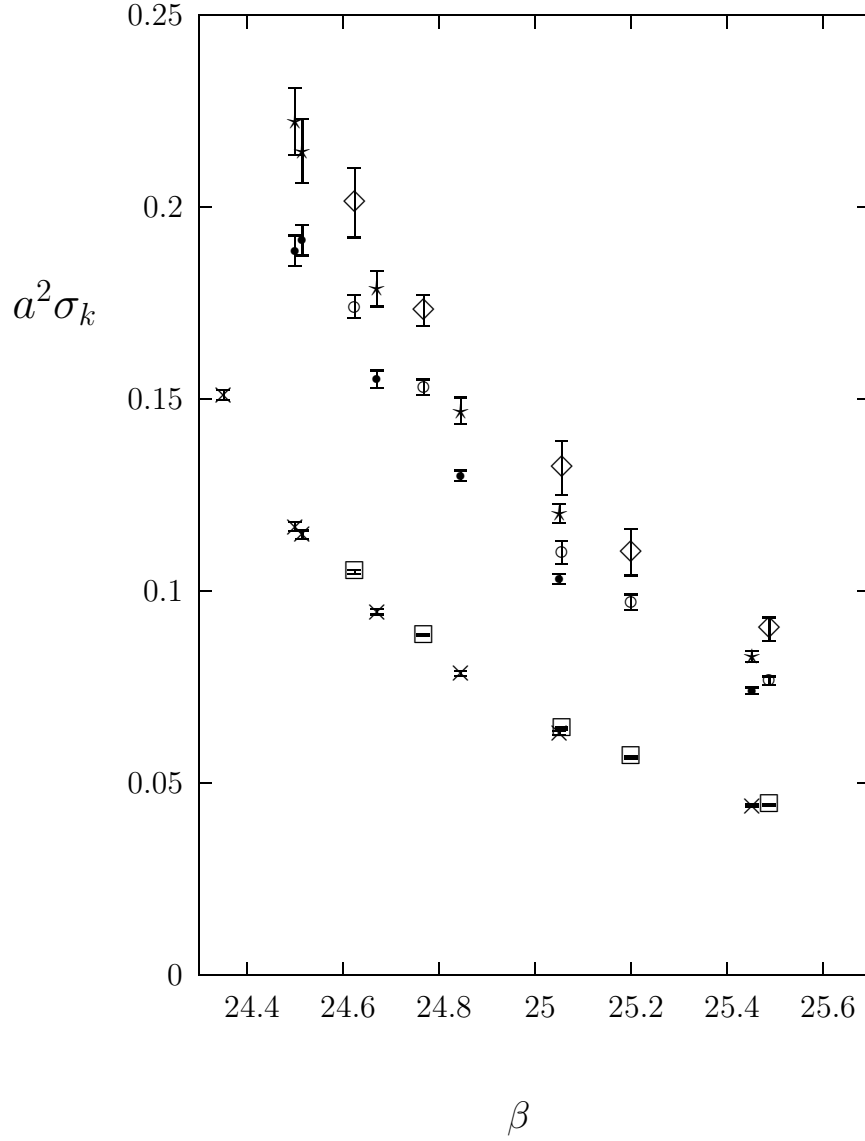


Figure 9: Comparison of the SU(6)  $k = 1$ ,  $k = 2$  and  $k = 3$  string tensions obtained in this work ( $\times$ ,  $\bullet$ ,  $\star$  respectively) with those obtained in [10] ( $\square$ ,  $\circ$ ,  $\diamond$  respectively). Plotted against the inverse coupling  $\beta$ .

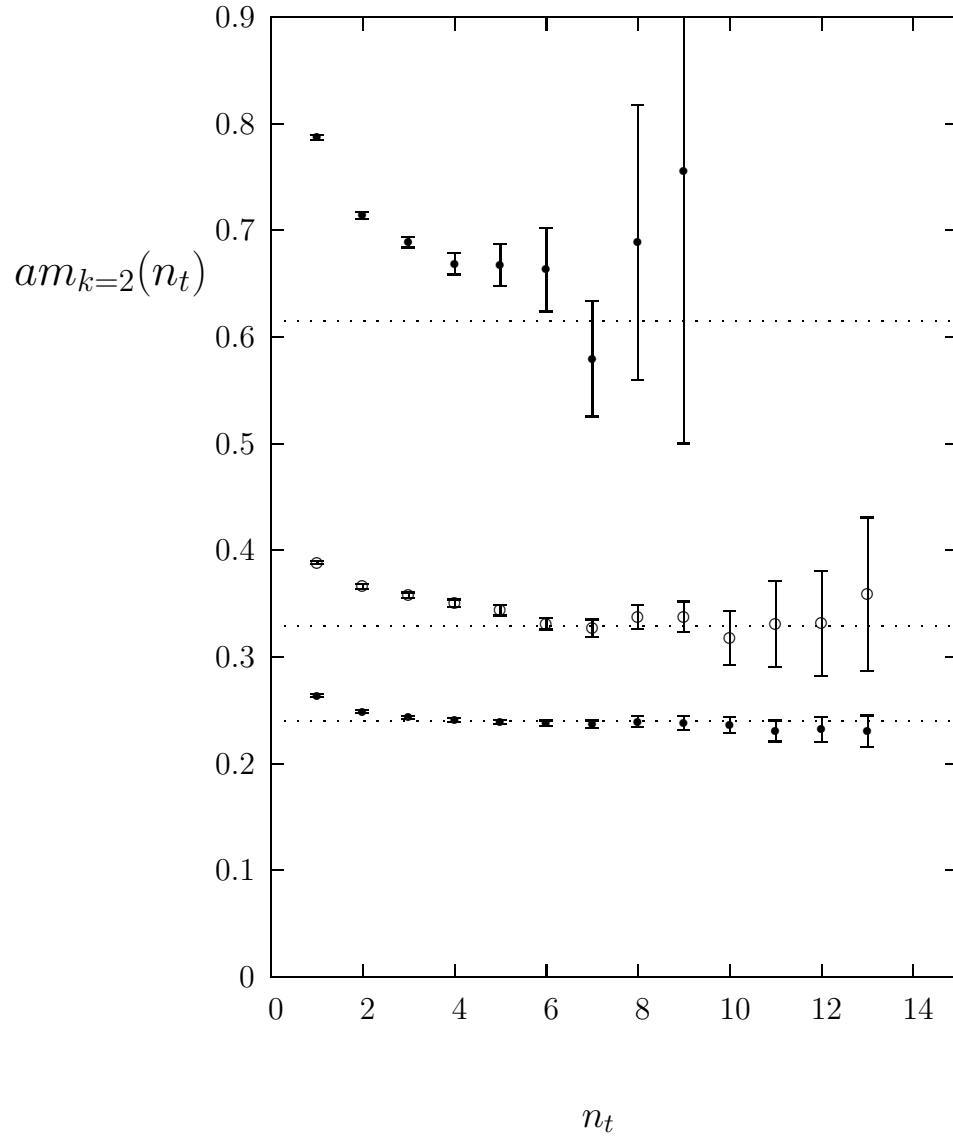


Figure 10: Effective mass of the  $SU(4)$   $k$ -string as a function of  $n_t$  from the  $16^3 40$  anisotropic lattice calculation with the smallest lattice spacing. The mass of the lightest string, in the fundamental representation,  $\bullet$ , and the lightest masses in the  $k = 2$  totally antisymmetric,  $\circ$ , and the  $k = 2$  symmetric,  $\bullet$ , representations, are shown. Dashed lines indicate the best mass estimate of the  $k = 1$  string, and the masses that one would then expect for the (anti)symmetric  $k = 2$  strings if one scales up the  $k = 1$  tension by the Casimir Scaling factor.

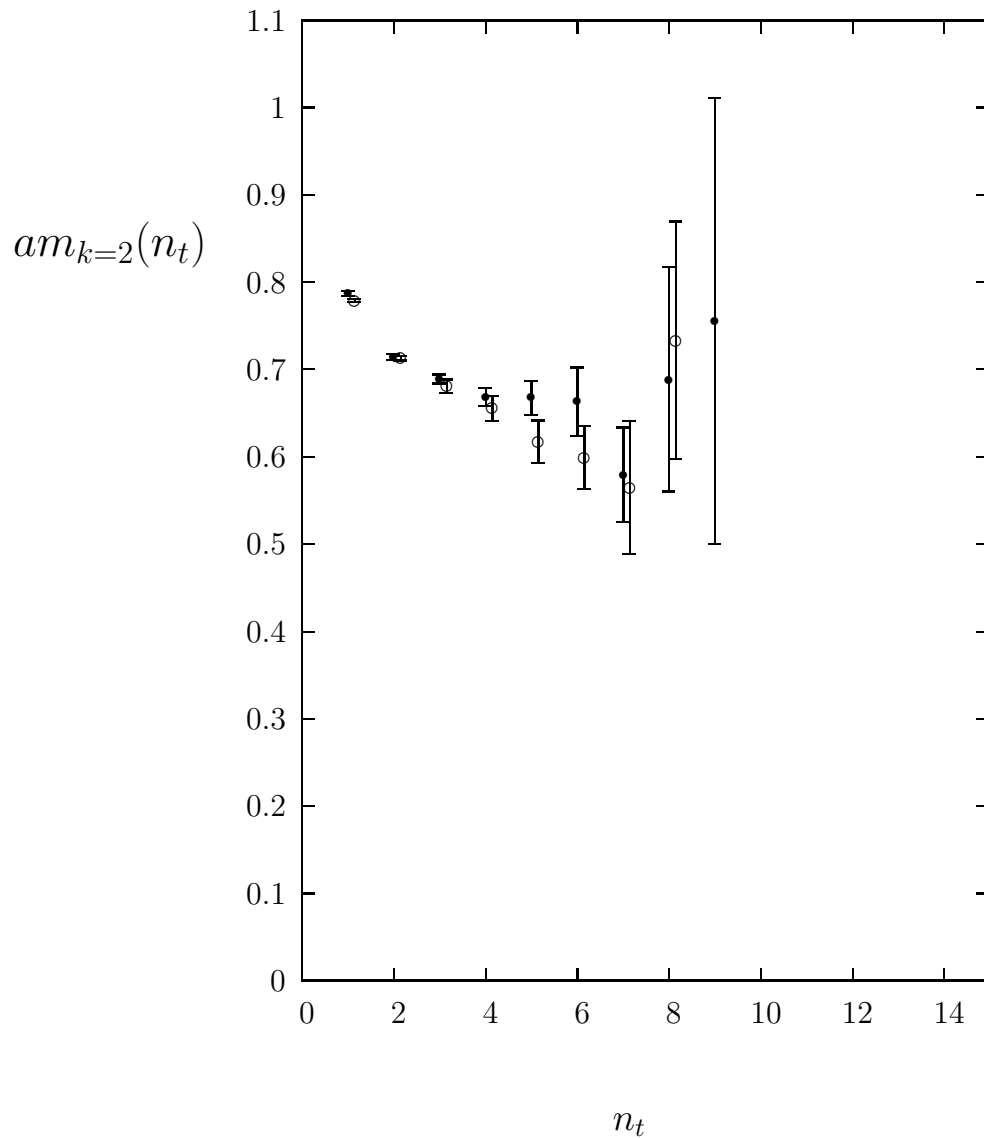


Figure 11: Effective mass of the SU(4)  $k = 2$  string as a function of  $n_t$  for the  $16^3 40$  anisotropic lattice with the smallest lattice spacing. We plot the lightest string mass in the totally symmetric  $k = 2S$  representation,  $\bullet$ , and the first excited mass in the totally antisymmetric  $k = 2A^*$  representation,  $\circ$ .

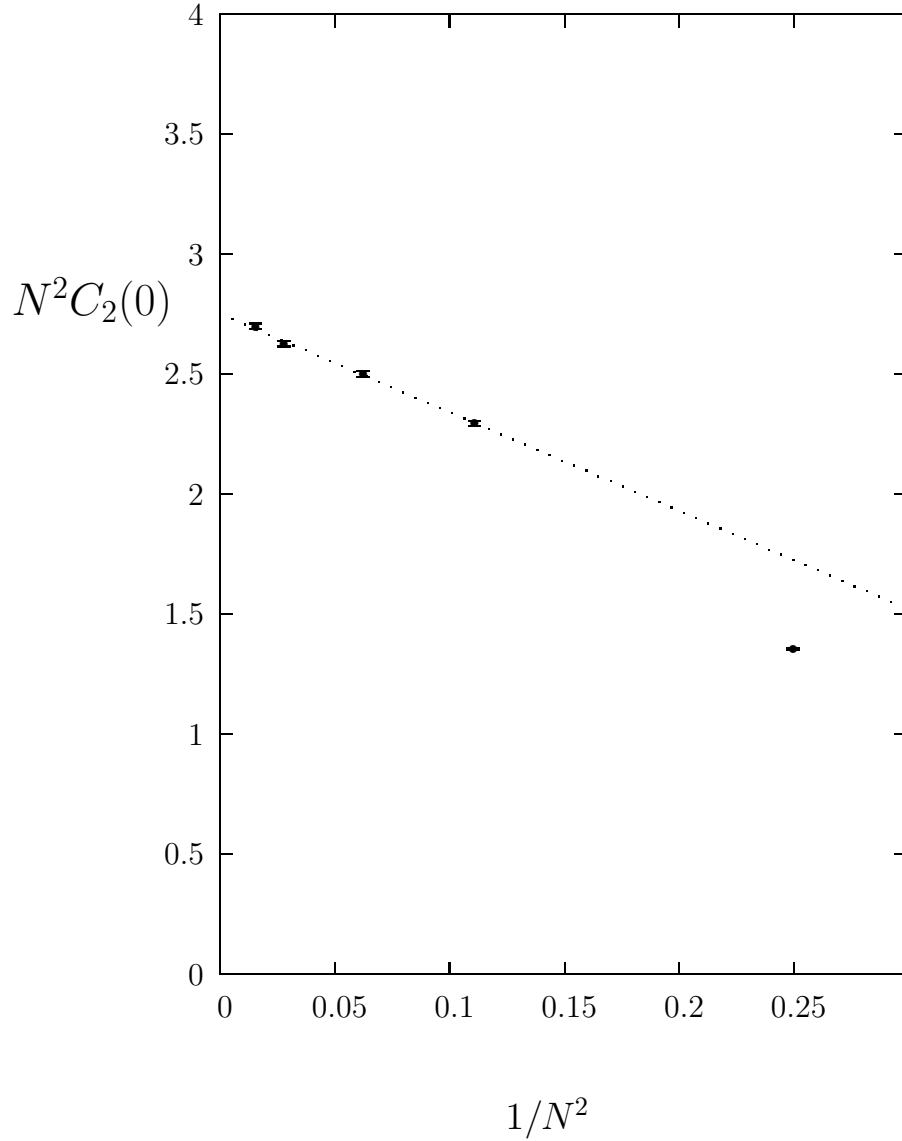


Figure 12: The  $N$ -dependence of the two point correlation function,  $C_2(t)$ , defined in eqn(35). The calculations are on  $10^4$  lattices at fixed lattice spacing,  $a \simeq 1/5T_c$ .

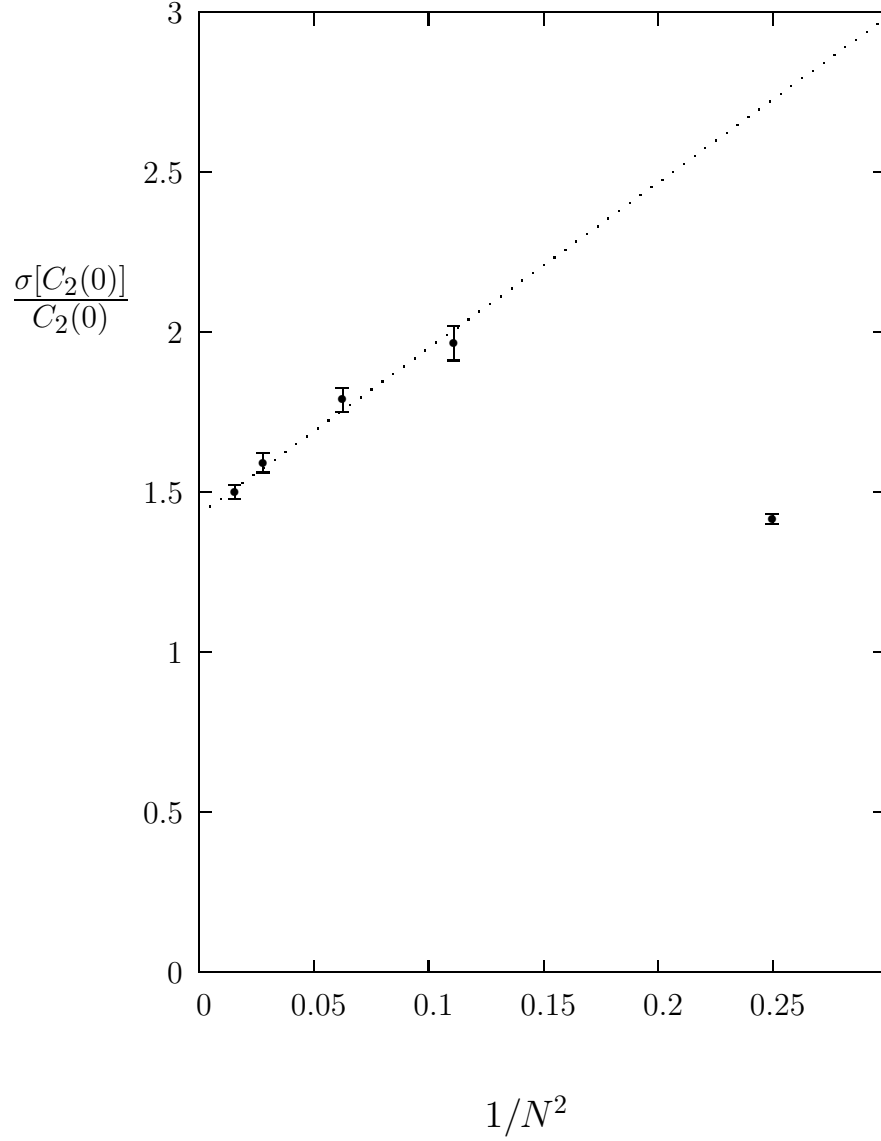


Figure 13: The fluctuation on the two point correlation function  $C_2(t)$  defined in eqns(35 - 40). The  $N$ -dependence on  $10^4$  lattices at fixed lattice spacing,  $a \simeq 1/5T_c$ .

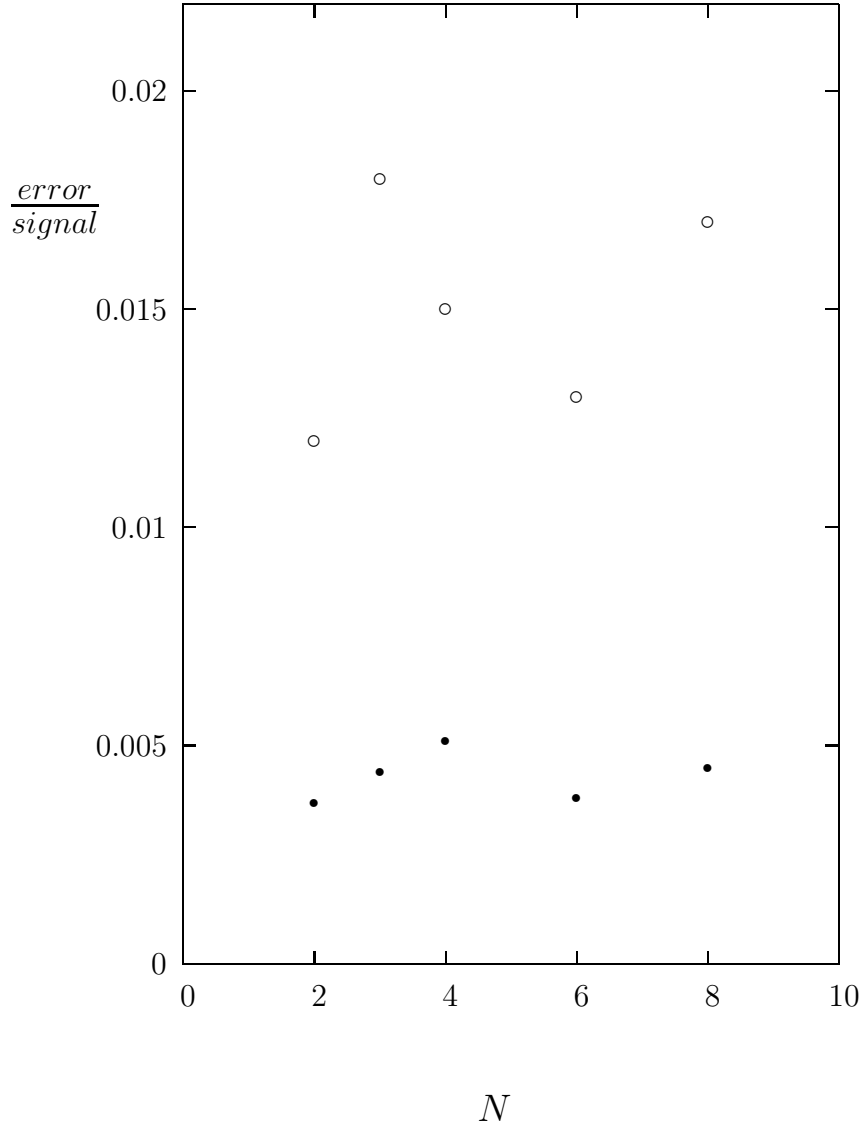


Figure 14: The  $N$ -dependence of the error to signal ratio for the two point correlation function,  $C_2(t)$ , defined in eqns(35 - 40) after  $10^5$  sweeps on  $10^4$  lattices at fixed lattice spacing,  $a \simeq 1/5T_c$ . For  $t = 0$  ( $\bullet$ ) and  $t = a$  ( $\circ$ ).

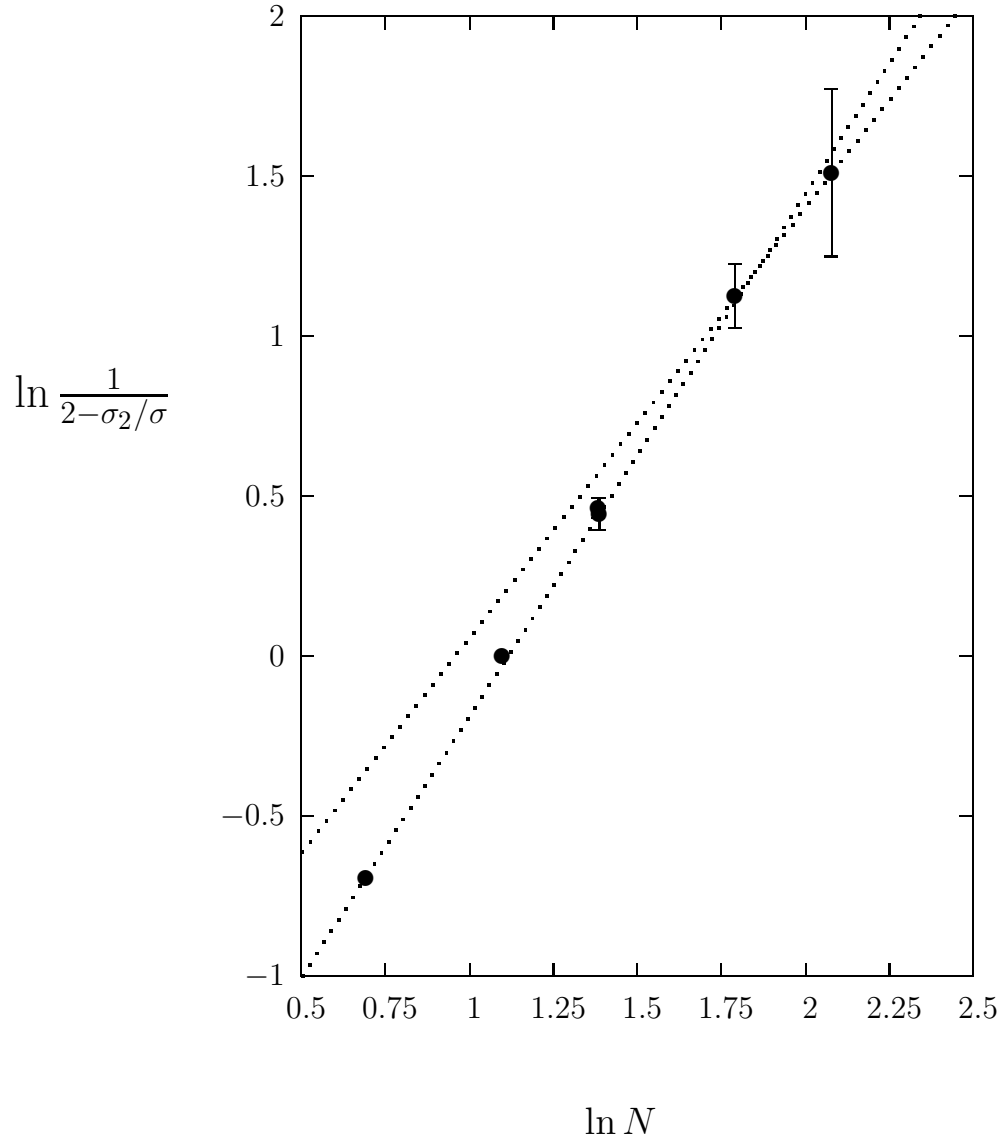


Figure 15: The calculated ratio  $\sigma_{k=2}/\sigma$  for  $N = 4, 6, 8$ , plotted so that the slope gives the power,  $\alpha$ , of the correction to the  $N = \infty$  limit if that is parameterised as  $1/N^\alpha$ . (We also show the ‘trivial’ values for  $N = 2, 3$ .) The best fits for  $N \geq 4$  and  $N \geq 6$  are shown.